CHAPTER 5

Principles of Laser Microdissection and Catapulting of Histologic Specimens and Live Cells

Alfred Vogel,[*] Verena Horneffer,[*] Kathrin Lorenz,[*] Norbert Linz,[*] Gereon Hüttmann,[*] and Andreas Gebert[†]

[*]Institute of Biomedical Optics, University of Lübeck
Peter-Monnik Weg 4, D-23562 Lübeck, Germany

[†]Institute of Anatomy, University of Lübeck
Ratzeburger Allee 160, D-23538 Lübeck, Germany

I. Introduction
II. Features of the Microbeam System and Materials Used
III. Dissection and Catapulting of Histologic Specimens
    A. Mechanism of Dissection
    B. Catapulting with Focused and Defocused Laser Pulses
    C. Possible Side Effects and Their Minimization
IV. Dissection and Catapulting of Live Cells
    A. Dissection in a Liquid Environment
    B. Catapulting of Live-Cell Populations
    C. Possible Side Effects and Their Minimization
V. Conclusions and Outlook
    A. Potential Improvements for Dissection
    B. Potential Improvements for Catapulting
References

Rapid contact- and contamination-free procurement of specific samples of histologic material for proteomic and genomic analysis as well as separation and transport of living cells can be achieved by laser microdissection (LMD) of the sample of interest followed by a laser-induced forward transport process [laser pressure "catapulting," (LPC)] of the dissected material.

METHODS IN CELL BIOLOGY, VOL. 82

0091-679X/07 $35.00
DOI: 10.1016/S0091-679X(06)82005-4

We investigated the dynamics of LMD and LPC with focused and defocused laser pulses by means of time-resolved photography. The working mechanism of microdissection was found to be plasma-mediated ablation. Catapulting is driven by plasma formation, when tightly focused pulses are used, and by ablation at the bottom of the sample for moderate and strong defocusing. Driving pressures of several hundred megapascals accelerate the specimen to initial velocities of 100–300 m/s before it is rapidly slowed down by air friction. With strong defocusing, driving pressure and initial flight velocity decrease considerably.

On the basis of a characterization of the thermal and optical properties of the histologic specimens and supporting materials used, we calculated the temporal evolution of the heat distribution in the sample. After laser microdissection and laser pressure catapulting (LMPC), the samples were inspected by scanning electron microscopy. Catapulting with tightly focused or strongly defocused pulses results in very little collateral damage, while slight defocusing involves significant heat and UV exposure of up to about 10% of the specimen volume, especially if samples are catapulted directly from a glass slide.

Time-resolved photography of live-cell catapulting revealed that in defocused catapulting strong shear forces originate from the flow of the thin layer of culture medium covering the cells. By contrast, pulses focused at the periphery of the specimen cause a fast rotational movement that makes the specimen wind its way out of the culture medium, thereby undergoing much less shear stresses. Therefore, the recultivation rate of catapulted cells was much higher when focused pulses were used.

I. Introduction

Procurement of specific samples of histologic material for proteomic and genomic analysis has become important with the increasing refinement of analytic techniques. Moreover, separation and transport of living cells is of interest for stem cell research, organ culture, or tissue engineering. Mechanical separation techniques are tedious, time consuming, and bear the risk of contamination. Therefore, faster laser-based processes have been developed (Eltoum *et al.*, 2002; Kehr, 2003; Thalhammer *et al.*, 2003), and several companies are active in this field. A widespread, rapid, contact- and contamination-free separation method consists in laser microdissection (LMD) of the sample of interest followed by a laser-induced forward transport process, which has been coined laser pressure ''catapulting'' (LPC) of the dissected material into the vial used for further analysis (Schütze and Lahr, 1998; Schütze *et al.*, 1998). This two-step procedure, consisting of laser microdissection and laser pressure catapulting (LMPC), is illustrated in Fig. 1. The scheme in Fig. 1 shows a setup with an inverted microscope but the same principle, with opposite direction of material transport, has been applied also for upright microscopes (Elvers *et al.*, 2005).

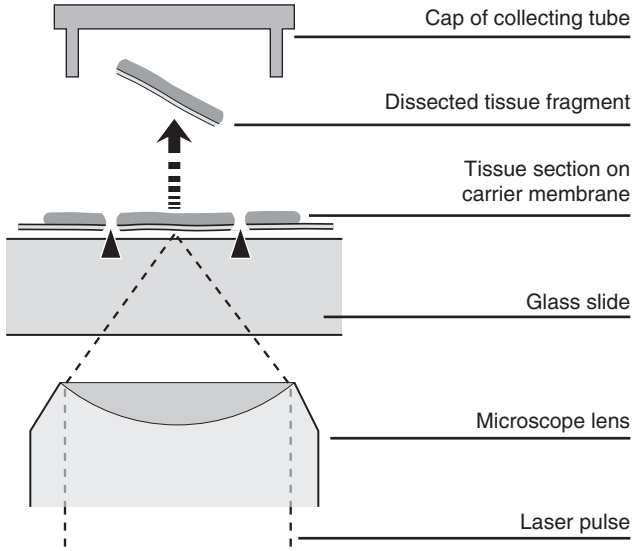

Fig. 1 Principle of separation of small biological objects, exemplified by the isolation of parts of a histologic section. The section is placed on a thin, UV-absorbing polymer foil that is mounted on a routine microscope glass slide. A region of interest is dissected from the section using a series of focused UV-A laser pulses (LMD) and subsequently catapulted (LPC) into the cap of a microfuge tube by a final, often more energetic, laser pulse. The catapulting pulse can be directed either in the center or in the periphery of the dissected specimen.

Historical roots of the individual steps of the process date about 30–40 years back. Soon after the first textbook on materials processing by high-power laser radiation appeared (Ready, 1971), LMD of histologic material using a UV-A laser was introduced in 1976, but the "harvesting" still had to be done with mechanical tools (Isenberg *et al.*, 1976; Meier-Ruge *et al.*, 1976). Ten years later, high-energy laser pulses were used to accelerate metallic flyers to velocities greater than 2.5 km/s for impact studies (Sheffield *et al.*, 1986), and present suggestions to exploit the potential of laser "catapulting" reach from the transfer of semiconductor devices in electronic circuit board manufacture (Mathews *et al.*, 2006) as far as to laser launching of objects into low Earth orbit (Phipps *et al.*, 2000). The underlying physical processes of laser-induced material transport were analyzed, among others, by Anderholm (1970), Fairand and Clauer (1979), Phipps *et al.* (1988, 2000), Romain and Darquey (1990), Fabbro *et al.* (1990), and Bäuerle (2000). Biologists became aware of the potential of laser catapulting in the late 1990s when Schütze and coworkers discovered that a combination of LMD and LPC with focused low-energy pulses can be used to isolate minute amounts of biologic material (Lahr, 2000; Schütze and Lahr, 1998; Schütze *et al.*, 1998). At the same time, a UV-absorbing polymer carrier foil was introduced to enhance the

laser light absorption in the specimen and to maintain its mechanical integrity during LPC (Schütze and Lahr, 1998). These advancements, together with an increased demand for separation techniques due to the refinements of proteomic and genomic analysis, and the proof that LMPC is compatible with DNA and RNA recovery (Schütze and Lahr, 1998) paved the way of LMPC into the market (www.PALM-Microlaser.com).

The next step ahead consisted of the development of a protocol for live-cell catapulting and recultivation (Hopp *et al*., 2005; Mayer *et al*., 2002; Stich *et al*., 2003). In parallel, the analysis of the dissection and catapulting mechanisms of biological material progressed. Cell surgery (Amy and Storb, 1965; Berns *et al*., 1969, 1971; Bessis *et al*., 1962; König *et al*., 1999, and references in Vogel *et al*., 2005a) and LMPC had been developed largely on an empirical basis. After it had been conjectured for a while that microdissection with pulse durations of nanoseconds or shorter is plasma-mediated (Greulich and Pilarczyk, 1998; Meier-Ruge *et al*., 1976), this hypothesis was experimentally proven in 2002 (Venugopalan *et al*., 2002), and a detailed theory of plasma-mediated nanosurgery of cells and tissues with femtosecond (fs) pulses was presented in 2005 (Vogel *et al*., 2005a). In the same year, it was shown that LMD and LPC of histologic material using focused UV nanosecond (ns) laser pulses are also plasma-mediated (Vogel *et al*., 2005b), and demonstrated that LPC can be performed using both focused and strongly defocused beams (Vogel *et al*., 2005b). With defocused beams, no plasma is formed, and the catapulting relies on ablation at the bottom of the catapulted sample. Elvers *et al*. (2005) proved that the LPC mechanism applies not only for the separation technique based on an inverted microscope but also for schemes using an upright microscope (www.leica-microsystems.com).

Besides LMPC, a number of related laser-based separation and transport techniques have been developed throughout the past 10 years. Emmert-Buck *et al*. (1996) introduced a laser capture technique in which a thin clear membrane is melted by an IR microbeam onto a small region of the histologic sample. The melted membrane sticks to the cells to be isolated, which can then be lifted and collected in a microfuge tube. This method was later refined by UV laser dissection of the region of interest before the tissue sample is harvested via IR laser-induced adhesion to a membrane (www.arctur.com) or via a specific membrane adhesion cap (www.molecular-machines.com). Laser-induced cell lysis combined with rapid transport of the lysed cell constituents for time-resolved capillary electrophoresis has been established by Allbritton and coworkers (Meredith *et al*., 2000; Sims *et al*., 1998), and the mechanisms of this technique were explored by Rau *et al*. (2004, 2006). Deposition of biomaterial films by a matrix-assisted pulsed laser evaporation method (MAPLE direct-write) was demonstrated by Chrisey *et al*. (2003), Wu *et al*. (2003), and Christescu *et al*. (2004). Serra *et al*. (2004) demonstrated the preparation of functional DNA micoarrays through laser-induced forward transfer by means of a titanium dynamic release layer and analyzed its mechanisms (Colina *et al*., 2006). MAPLE direct-write was used also to create three-dimensional (3D) heterogeneous cell patterns that are of interest for tissue engineering (Barron *et al*., 2004; Ringeisen

et al., 2004; Wu *et al.*, 2003). While the above work was performed utilizing ns laser pulses (mostly at UV wavelengths), several researchers employed fs pulses for biofilm and DNA printing (Karaiskou *et al.*, 2003; Zergioti *et al.*, 2005) and shock wave induced cell isolation, (Hosokawa *et al.*, 2004). Laser-induced forward transfer with fs pulses was found to be more directional than with ns pulses (Zergioti *et al.*, 2003).

The present study focuses on the investigation of LMD and LPC using UV ns laser pulses because this technique is widely used in many laboratories. It is the goal to elucidate the mechanisms and potential side effects of LMPC in both dry and liquid environments (i.e., for histologic specimens and living cells). On the basis of this analysis, strategies for an improvement of the two techniques will be discussed.

II. Features of the Microbeam System and Materials Used

We used a PALM microbeam system equipped with an N_2 laser ($\lambda = 337$nm) emitting pulses of 3-ns (FWHM) duration. The laser beam is coupled into an inverted microscope (Zeiss Axiovert 200) with a motorized, computer-controlled stage. The microscope objectives used in this study were Zeiss LD Plan-Neofluar 40×/0.6 corr, Plan Neofluar 20×/0.5, Fluar 10×/0.5, and Fluar 5×/0.25. The UV-absorbing polymer foil mounted on the glass slides carrying the histologic sections (Fig. 1) consists of polyethylene naphthalate (PEN) and is 1.35-μm thick.

An energy calibration (Fig. 2) showed that the relation between the setting at the control box and the actual energy transmitted through the objectives is logarithmic. The transmitted energy is largest for objectives with small magnification because

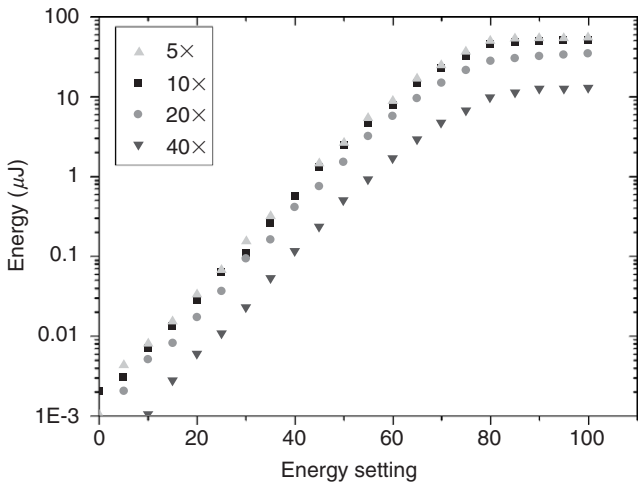

Fig. 2 Pulse energy transmitted through the microscope objectives for different settings at the laser control box of the PALM microbeam in semilogarithmic representation.

they possess large optical pupils that transmit the laser beam with little or no vignetting. The focal spot sizes were measured using a knife-edge technique, as described by Sasnett (1989) and Siegmann *et al.* (1991). The result for the 40× objective is shown in Fig. 3A. Because of the poor quality of the N_2 laser beam (Fig. 3B and C), the spot diameter (4.2 μm up to $1/e^2$ irradiance values) is more than six times larger than the diffraction limited focus diameter. Nevertheless, the hot spot visible in the center of the far-field beam profile in Fig. 3C allows to produce relatively fine effects if energies very close to the ablation threshold are employed. In the present generation of microbeam systems, the N_2 laser has been replaced by a frequency-tripled Nd:YAG laser emitting at $\lambda = 355$ nm that exhibits

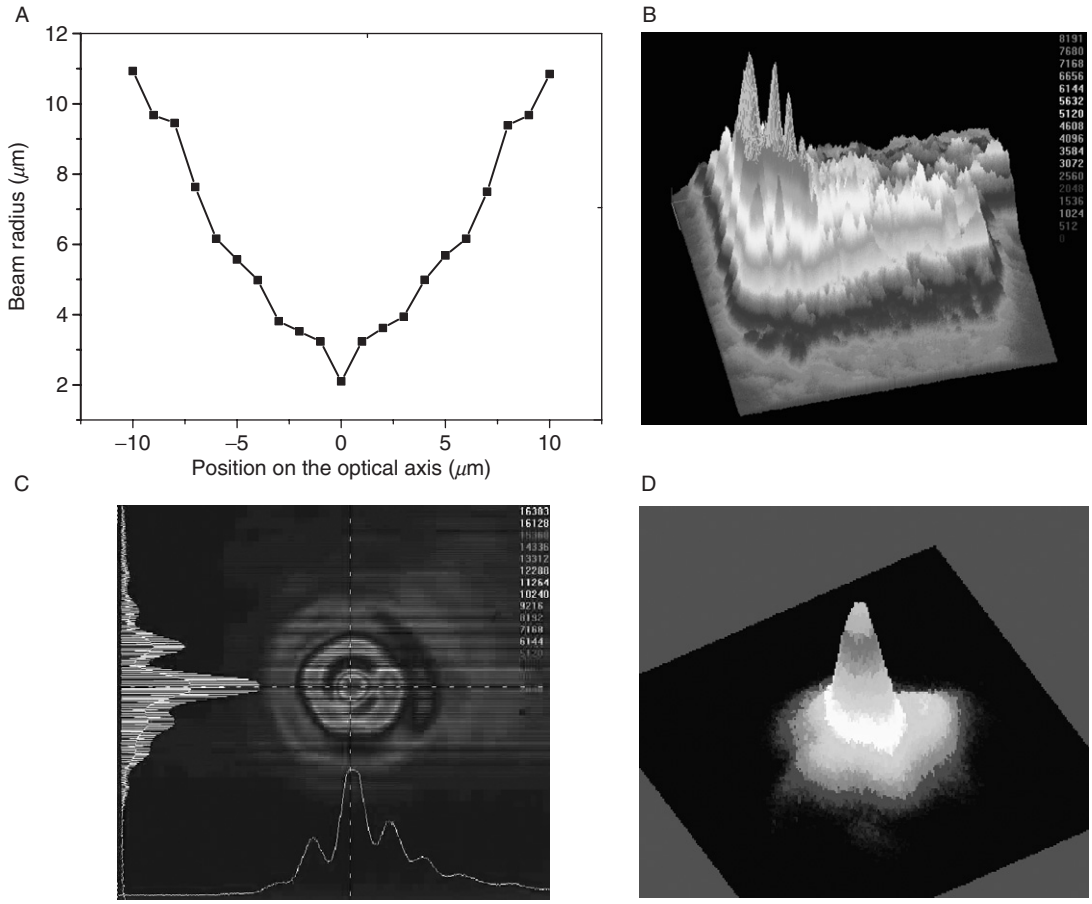

Fig. 3 (A) Spot size of the N_2 laser beam focused through the 40× objective, (B) near field and (C) far-field profiles of the N_2 laser beam, and (D) far-field beam profile for the frequency-tripled Nd:YAG laser.

a much better beam profile, as shown in Fig. 3D, and thus makes it possible to achieve a nearly diffraction limited focal spot size.

The transmission at $\lambda = 337\,\text{nm}$ of cells, histologic material, and the polymer foils mounted below the histologic sections were measured in the microbeam setup using an Ophir PD10 detector with 1-nJ sensitivity and in a spectral photometer. All measurements were performed at low irradiance where nonlinear absorption is negligible. The measurements on the optical properties of the cultured cells [Chinese hamster ovary (CHO) cells] were performed on a single, confluent cell layer. The determination of the optical properties of the PEN foil required measurements with an integrating sphere, since PEN scatters strongly at $\lambda = 337\,\text{nm}$. For PEN, we measured total transmission and reflection as described by Vogel *et al.* (1991), and calculated the absorption coefficient μ_a and scattering coefficient μ_s using the Kubelka Munk theory (Cheong *et al.*, 1990; Star *et al.*, 1988). The effective attenuation coefficient μ_{eff} and optical penetration depth δ were then obtained by means of the relation (Jacques, 1993):

$$\delta = \frac{1}{\mu_{\text{eff}}} = \frac{1}{\{3\mu_a[\mu_a + \mu_s(1 - g)]\}^{1/2}} \tag{1}$$

assuming a value of $g = 0.5$ for the scattering anisotropy coefficient that is representative for moderate forward scattering in single scattering events (Cheong *et al.*, 1990).

The heat capacity of the polymer foil and the histologic specimens were determined by differential scanning calorimetry (DSC) in comparison with a sapphire standard, and the dissociation temperatures were obtained through thermogravimetric analysis (TGA), that is, by measuring the weight loss as a function of temperature. As an example, Fig. 4 shows the DSC and TGA data for PEN foil, the polymer material mounted on microscope glass slide on which the histologic specimens are usually placed. Table I presents a summary of the measurement results for the optical and thermal material properties of materials relevant for LMD and LPC of cells and histologic materials.

III. Dissection and Catapulting of Histologic Specimens

A. Mechanism of Dissection

It has been shown recently that cell surgery using pulsed visible and near-IR irradiation is plasma mediated, that is, based on nonlinear absorption via multiphoton and avalanche ionization. The irradiances required for cell surgery with ns laser pulses are $\sim 10^9$ W/mm^2, just as the optical breakdown threshold in water (Venugopalan *et al.*, 2002). For fs laser pulses, both the required irradiance for dissection and the threshold irradiance for optical breakdown in water are about two orders of magnitude larger while the breakdown energy is about three orders of magnitude smaller (Vogel *et al.*, 2005a).

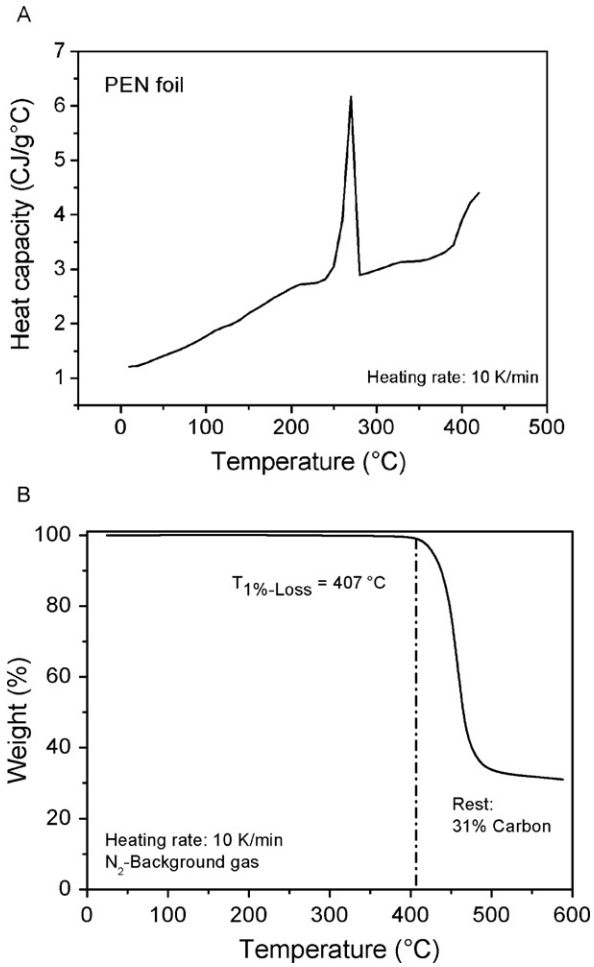

Fig. 4 Thermal properties of PEN foil. (A) Temperature-dependent heat capacity C_p. The peak at 269 °C indicates an endothermal melting transition, and the rise above 400 °C is due to dissociation. (B) Temperature-dependent weight loss for a slow heating rate, with dissociation starting at 407 °C and ending at ≈500 °C. The dissociation temperature defined by half of the total weight loss is ≈450 °C. For very fast heating rates such as in pulsed laser catapulting, it will probably be higher because dissociation is a rate process that depends on both temperature and time.

The dominant role of plasma formation for cell surgery using visible or near-IR wavelengths is not surprising because the linear absorption of water and biomolecules in this region of the optical spectrum is very small (Litjens *et al.*, 1999; Vogel and Venugopalan, 2003). Our present study revealed that plasma formation plays a key role also for the dissection of cells at UV-A wavelengths. Although the absorption increases with decreasing wavelength, it is still fairly small at $\lambda = 337\,\text{nm}$

Table I
Optical Properties at 337 nm and Thermal Properties of Cells, Histologic Material, Polyethylene Naphthalate (PEN) Polymer Foil, Glass, and Water

Material	Sample thickness × (μm)	Transmission (%)	Extinction coefficient μ_{eff} (cm^{-1})	Optical penetration depth δ (μm)	Average heat capacity (kJ/K/kg)	Dissociation temperature (°C)	Heat conductivity (W/m/K)	Density (W/m*K)
Glass slide	1000	94.7	0.55	18,200	0.666	–	1.07	2500
PEN-foil	1.35	$T = 20.5$ $R = 22.4$	$\mu_a = 3{,}520$ $\mu_s = 17{,}370$ $\mu_{eff} = 11{,}360$	0.88	2.7	460	≈0.4	1.39
Teflon foil	≈25	95.8	17.2	580	1.0	–	≈0.2	2200
H&E-stained histol. specimen	≈5	7–35(15.7)	2100–5300 (3700)	1.9–4.8(2.7)	3.2	340	≈0.5	≈1000
CHO cells	≈5	93.8	127	79	4.0	150–300		≈1000
Water			0.0172	5.8×10^5	4.187	300	0.598	998

All transmission data are corrected for specular reflection, that is, they represent purely the transmission of the sample. The optical parameters for stained histologic specimen cover a certain range given by variations in staining. The values in brackets were used for the temperature calculation is Section III.C.1. Sources for data not measured in this study are water absorption, Litjens *et al*. (1999); heat conductivity, heat capacity, and density of water, glass, PEN, and Teflon, Kuchling (1991); density of PEN, www.m-petfilm.com. The dissociation temperature of water corresponds, in the present context, to the superheat limit in bubble-free liquid water (Vogel and Venugopalan, 2003), and the dissociation temperature of cells corresponds to their heterogeneous nucleation threshold (Neumann and Brinkmann, 2005; Simanowski *et al*., 2005).

(the optical penetration depth is about 80 μm, see Table I) and even smaller at 355 nm. Therefore, the ablation threshold in unstained cells was found to be only slightly smaller than the threshold for the formation of luminescent plasma, as shown in Fig. 5A.

Stained histologic specimens and the PEN polymer foil have a much larger optical absorption coefficient than unstained cells (see Table I). For these materials, the ablation threshold is thus considerably lower than the plasma formation threshold (Fig. 5A). It has previously been speculated that ablation of biomaterial at the N_2 laser wavelength of 337 nm is based on photochemical dissociation (Schütze and Lahr, 1998). However, this is unlikely because indications for a relevant contribution of photochemical effects to ablation have been found only at much shorter wavelengths, for example with ArF laser pulses at $\lambda = 193$ nm while they were completely absent with XeCl excimer laser pulses of 308-nm wavelength (Vogel and Venugopalan, 2003). Therefore, we assume that ablation based on linear absorption at $\lambda = 337$ nm is a purely thermal process.

Figure 5A indicates that dissection of histologic specimens by N_2 laser pulses could, in principle, be performed by ablation without any contribution of plasma

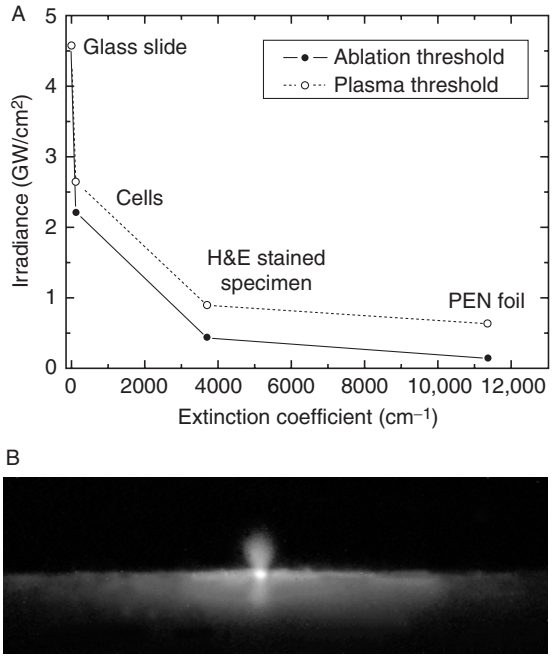

Fig. 5 (A) Thresholds for ablation and plasma formation at 337 nm for various materials. (B) Image of plasma luminescence during microdissection of histologic specimens (6 pulses of 4.6 μJ). The plasma luminescence is blue at the target surface but turns red at larger distances where the temperatures are smaller and the corresponding wavelength of blackbody radiation is longer. The blue light emission adjacent to the laser focus is caused by fluorescence of the PEN polymer foil.

formation because the ablation threshold (0.15 μJ with NA = 0.6) is slightly lower than the threshold for plasma formation (0.3 μJ). However, because of the small ablation efficiency close to the threshold for material removal this dissection mode would require very many pulses which are not viable at the relatively small laser repetition rate of 30 Hz. Therefore, pulse energies of about 0.5 μJ are commonly used and focused through a 40×, NA = 0.6 microscope objective. That energy is larger than the threshold for plasma formation, and dissection is thus accompanied by blue plasma luminescence as visible in Fig. 5B. The slightly disruptive action of the plasma expansion helps to achieve clean cuts without any bridges remaining between the parts to be separated. We conclude that dissection of histologic specimens using UV laser pulses is based on plasma formation (i.e., nonlinear absorption) initiated by linear absorption.

B. Catapulting with Focused and Defocused Laser Pulses

1. Driving Forces for Catapulting with Focused Pulses

The mechanisms of catapulting of histologic specimens and live cells were analyzed by time-resolved photography. Similar techniques have been employed previously for the analysis of other laser-induced transport processes (Koulikov and Dlott, 2001; Lee *et al.*, 1992; Nakata and Okada, 1999; Papazoglou *et al.*, 2002; Rau *et al.*, 2004; Young *et al.*, 2001), and LPC by laser pulses focused through an upright microscope has been documented by high-speed cinematography with 1-ms interframing time (Elvers *et al.*, 2005). We achieved a temporal resolution better than 100 ns by using single frame photography with increasing time delay between catapulting laser pulse and the instant at which the photograph was exposed (Vogel *et al.*, 2007). The catapulted specimens were imaged in transillumination using the light of a plasma discharge lamp with 20-ns duration (Nanolite). The total magnification of the imaging system was 44×, and the images were detected using a 6-megapixel digital camera. The laser-produced pressure waves were visualized by means of a sensitive dark-field Schlieren technique (Vogel *et al.*, 2006). A frequency-doubled Nd:YAG laser beam coupled into a 300-m-long multimode fiber to destroy temporal coherence served as speckle-free light source for photography with 16-ns exposure time. To reduce the background noise and enhance the visibility of the laser-produced shock wave, a reference image was taken at time $t < 0$ and subtracted from each image recorded after the release of the catapulting laser pulse. The initial phase of the catapulting process was documented with time increments of 2–60 ns. The high time resolution allowed to deduce the laser-produced pressure from the speed of the resulting pressure waves (Lorenz, 2004; Vogel *et al.*, 1996b, 2007).

The specimen is usually located on a PEN foil backed by a transparent substrate (glass slide). Laser pulse energies commonly used for catapulting are larger than the energies employed for LMD that was already shown to rely on plasma formation. It is thus obvious that catapulting with focused laser pulse is driven by plasma

formation in the confined space between specimen and substrate. The initial catapulting dynamics under these conditions is shown in Fig. 6. The luminescent plasma driving the catapulting is visible in all frames. Immediately after the laser pulse, small debris particles are ejected with high velocity, and after 270 ns, the specimen is already clearly detached from the substrate surface. At the location of plasma

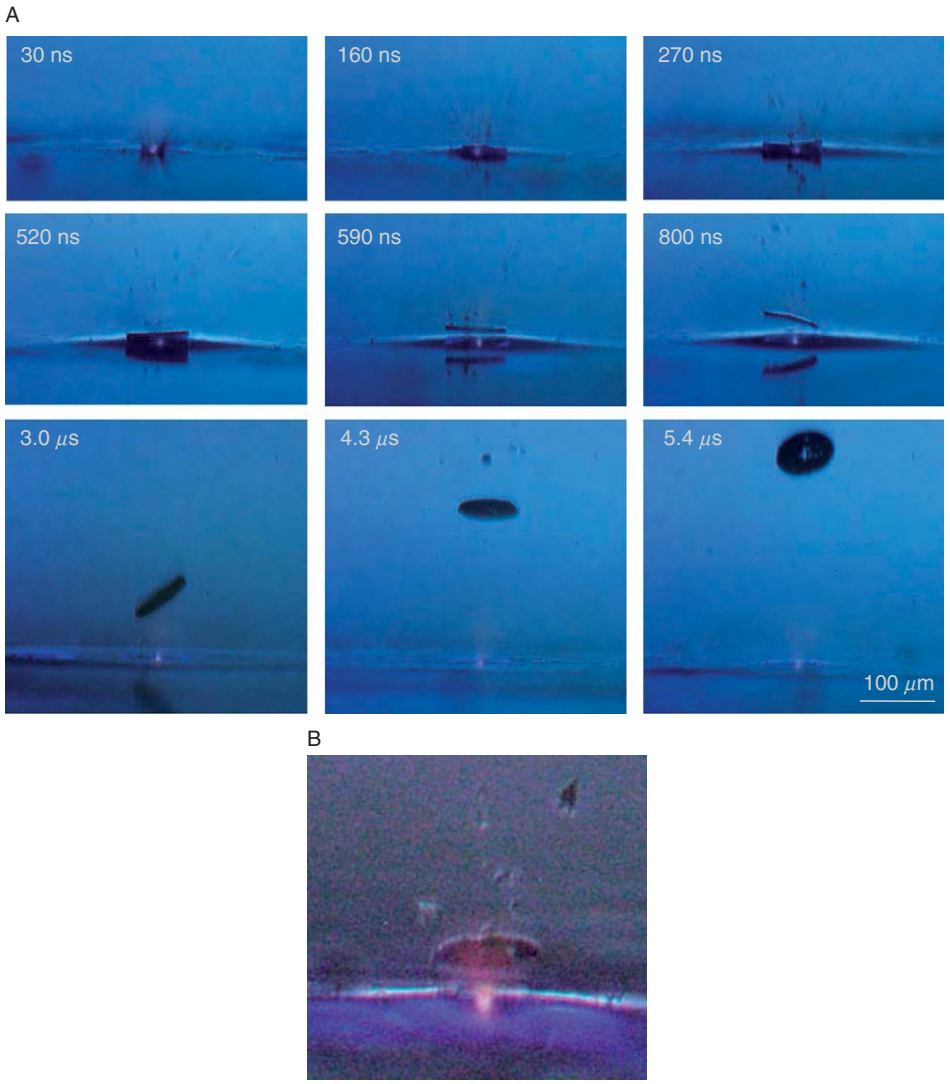

Fig. 6 (A) Initial phase of the catapulting dynamics of a specimen with 80-μm diameter from a paraffin section. 40× objective, NA = 0.6, and E = 10 μJ. (B) Enlarged view of the specimen after 1.7 μs showing the luminescent plasma driving the specimen, and the blue fluorescence of the PEN polymer foil.

formation, a hole is produced in the specimen, which is clearly visible in the image taken after 5.4 μs.

The pressure wave produced by the expansion of the laser plasma is shown in Fig. 7. An evaluation of the photographic series provided quantitative information on the propagation distance of the laser-produced pressure wave, the ejected debris, and the catapulted specimen as a function of time that is presented in Fig. 8. The initial velocity of the pressure wave amounts to 26,000 m/s, which is 76 times larger than the normal sound velocity in air and thus indicative for a strong shock wave. The plasma pressure driving the shock wave can be derived from the initial shock wave velocity v_s using the relation (Landau and Lifschitz, 1987):

$$p_{\text{plasma}} = \left[\left(\frac{7}{6}\right)\left(\frac{v_s}{c_0}\right)^2 - \left(\frac{1}{6}\right)\right] p_0 \tag{2}$$

Here $c_0 = 345$ m/s denotes the normal sound velocity in air and $p_0 = 0.1$ MPa is the atmospheric pressure. The initial laser-produced pressure was found to be 670 MPa, a typical value for plasmas generated in a confined geometry

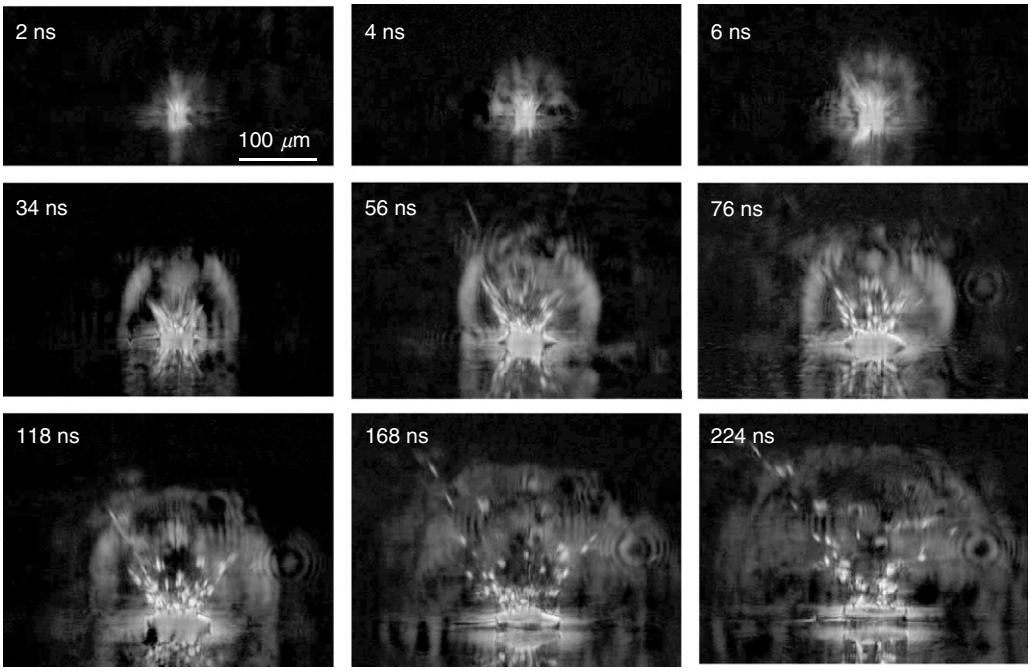

Fig. 7 Dark-field photographic series showing the first 225 ns of the catapulting dynamics. A specimen with 80-μm diameter from a paraffin section was catapulted using a 40× objective, NA = 0.6, and E = 10 μJ. The movement of the ejected particles and the propagation of the laser-induced shock wave can be recognized, followed by the detachment of the specimen after 100–200 ns.

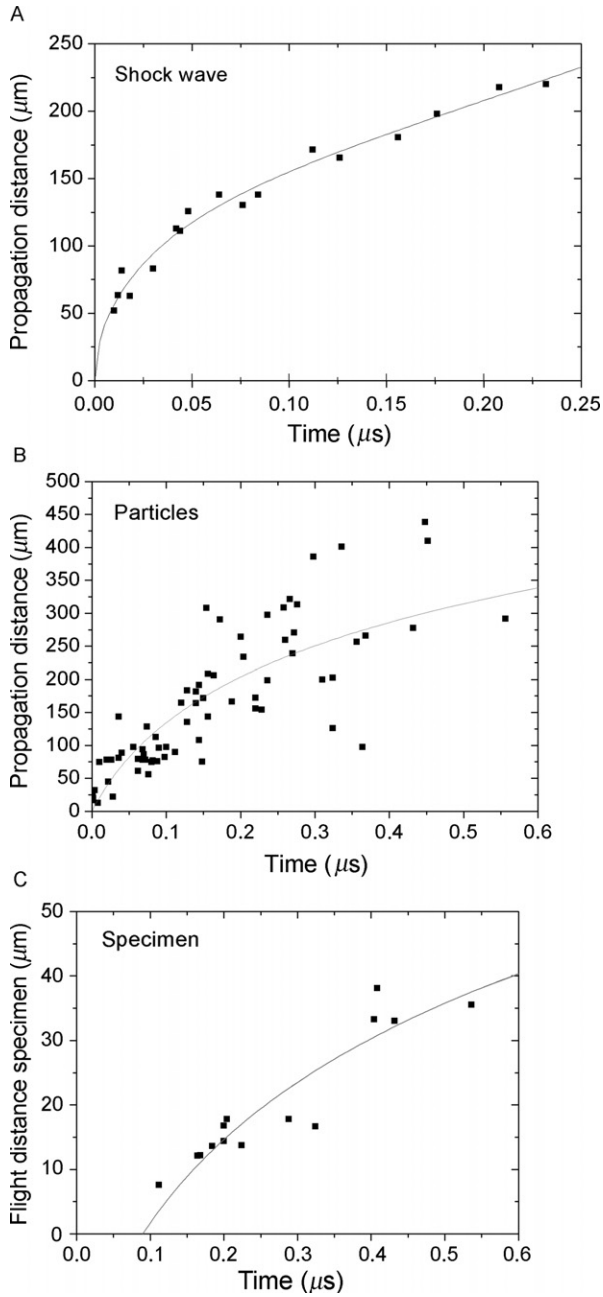

Fig. 8 Propagation distance of the laser-produced shock wave (A), the ejected particulate debris (B), and the catapulted specimen (C) as a function of time. From the slope of the d(t) curves, initial velocities of (A) 26,000 m/s, (B) 2200 m/s, and (C) 178 m/s can be deduced, which corresponds to (A) 76×, (B) 6.4×, and (C) 0.52× the sound velocity in air. 40× objective, NA = 0.6, specimen diameter 80 μm, and E = 10 μJ.

(Anderholm, 1970; Fabbro *et al*., 1990). Similar pressure values were also obtained by analyzing the acceleration of the debris flying off from the laser focus that is visible in the dark-field images of Fig. 7. Its peak velocity after a 10-μJ laser pulse is already reached at the end of the laser pulse (i.e., after 3 ns) and amounts to 2200 m/s (Lorenz, 2004).

The initial specimen velocity in Fig. 8C is ≈180 m/s. In the early days of LPC, it has been speculated that the specimens are driven by the light pressure (Schütze and Lahr, 1998). We can check the validity of this hypothesis by comparing the measured specimen velocity with the speed that can be imparted by the light pressure

$$p_{\text{light}} = \frac{I}{c} \tag{3}$$

Here I is the irradiance in the illuminated laser spot and c is the vacuum velocity of light. The accelerating force exerted by the light pressure acts during the laser pulse duration and the final velocity reached can be calculated considering the mass of the specimen. The calculation yields $v = 0.9$ mm/s for a specimen of 80-μm diameter, 7-μm thickness, and a mass density of 1 g/cm^3 that is catapulted by a 10-μJ pulse (parameters as in Fig. 8). This value is five orders of magnitude smaller than the actual velocity. The pressure exerted by the photons in the laser pulse, which is the working mechanism in laser tweezers (Ashkin, 1986; Greulich, 1999; Schütze and Clement-Sengewald, 1994), thus plays only a negligible role in LPC.

We showed that catapulting with focused pulses relies on the pressure produced by confined plasma formation. However, in spite of the large pressures involved, the catapulted specimens in Fig. 6 show little bending or other deformations. This is due to the fact that the large pressure at the focus is in vertical direction rapidly released by the hole formation in the specimen. In horizontal direction, the shock wave spreads across the specimen diameter within about 20 ns (Fig. 7). This way, it produces an approximately homogeneous elevated pressure below the specimen that lifts off from the substrate after about 100–200 ns (Figs. 6 and 7). In Fig. 6, one can see that the horizontal pressure wave also propagates under adjacent parts of the histologic section and transiently detaches them from the substrate for a few microseconds. The average pressure under the entire catapulted specimen during the acceleration phase of about 100 ns can be derived from the velocity reached after this phase, the acceleration time, and the estimated mass of the specimen (Lorenz, 2004). It amounts to about 18 MPa for the parameters in Fig. 8, which is considerably less than the peak pressure within the laser plasma of ≈670 MPa.

In some cases, the histologic specimens to be catapulted are mounted on a foil without backing by a glass substrate. Without confinement by the glass substrate, the plasma or ablation plume can freely expand. In this case, catapulting relies merely on the pressure produced by ablative recoil. Therefore, it is smaller than for plasma generation or ablation in a confined geometry, as shown in Fig. 9. The impulse coupling efficiency in laser ablation was theoretically analyzed by Phipps *et al*. (1988) and Dingus (1992, 1993). It was predicted to be smaller without

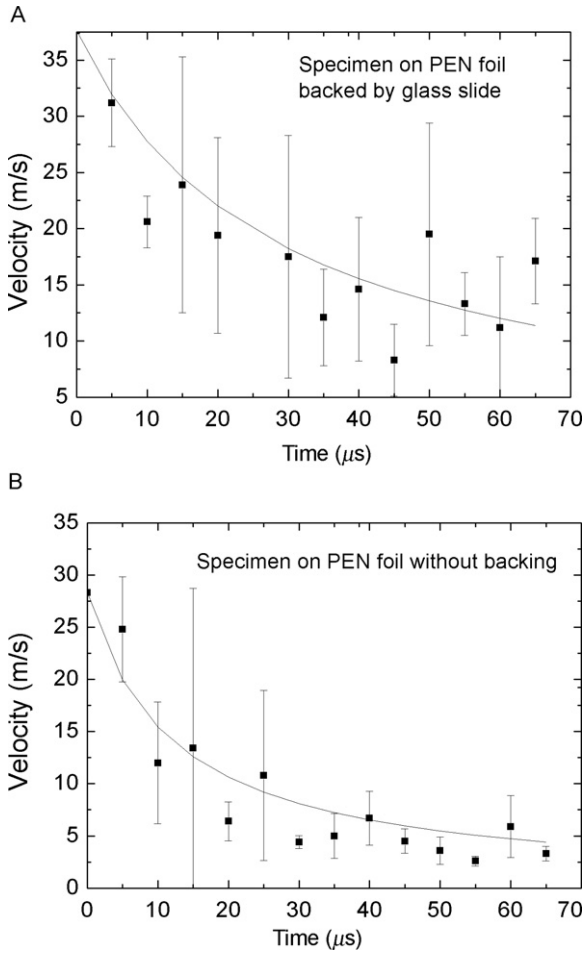

Fig. 9 Comparison of the velocities of specimens on a foil (A) with and (B) without backing by a glass substrate. Each data point refers to the average of five measurements. Specimen diameter 80 μm, 40× objective, NA = 0.6, and E = 5 μJ.

confinement of the ablation products, in agreement with our present observations and with results for aluminum foils obtained previously by Sheffield *et al.* (1966).

The dependence of the velocity on laser pulse energy for specimens that are backed by a glass slide is shown in Fig. 10. As expected, the specimen velocity increases monotonously with laser energy. In the energy range investigated, which is still close to the catapulting threshold, their relation is approximately linear. However, further above threshold we would rather expect a square root dependence corresponding to a constant conversion efficiency from laser energy into the kinetic energy of the moving specimen.

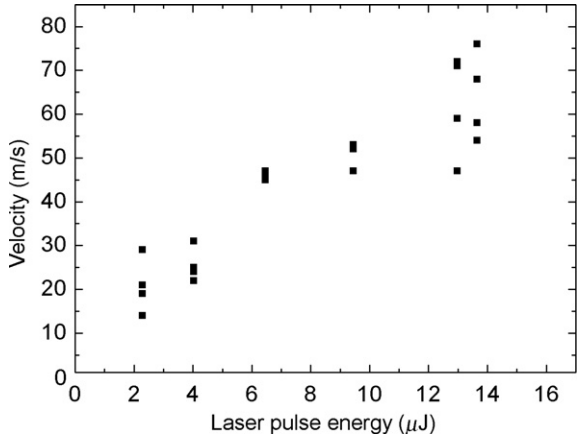

Fig. 10 Dependence of specimen velocity on laser pulse energy (average velocity values during the first 15-μs flight time). Specimens of 80-μm diameter were catapulted using a 40× objective and NA = 0.6.

For a constant laser energy of 10 μJ, the velocity of the dissectats was found to be 2.3 times larger when the laser pulses were focused through a 5× objective instead of a 40× objective. This striking difference is due to the fact that the focal spot size increases with decreasing numerical aperture (NA) of the objective. The measured focus radius of the N_2 laser beam in the PALM system was 21.4 μm for the 5×, NA = 0.25 objective compared to 2.1 μm for the 40×, NA = 0.6 objective. Because of the larger spot size, no holes were formed in the specimens during catapulting with the 5× objective, and the acceleration was faster due to the better confinement of the ablation products under the specimen.

2. Flight Trajectories of the Specimens

The catapulted specimen has to be accelerated against inertia and hydrodynamic drag. Acceleration ceases when the force exerted by the pressure below the specimen becomes smaller than the resistance originating from atmospheric pressure and hydrodynamic drag. Afterward, the specimens are slowed down by the air friction. The trajectory of the dissectats during their flight toward the microfuge cap is visible in the picture series in Fig. 11A and evaluated quantitatively in Fig. 11B.

A theoretical description of the flight trajectory $z(t)$ for the phase dominated by air friction is generally quite complicated (Elvers *et al.*, 2005; Jiménez *et al.*, 2005). However, for large particle velocities and sizes, Newtonian friction (related to the inertia of the displaced material) dominates Stokes friction (related to the medium viscosity), and it can be assumed that the hydrodynamic drag is approximately proportional to the square of the velocity. One then obtains the trajectory (Hibst, 1996; Jiménez *et al.*, 2005).

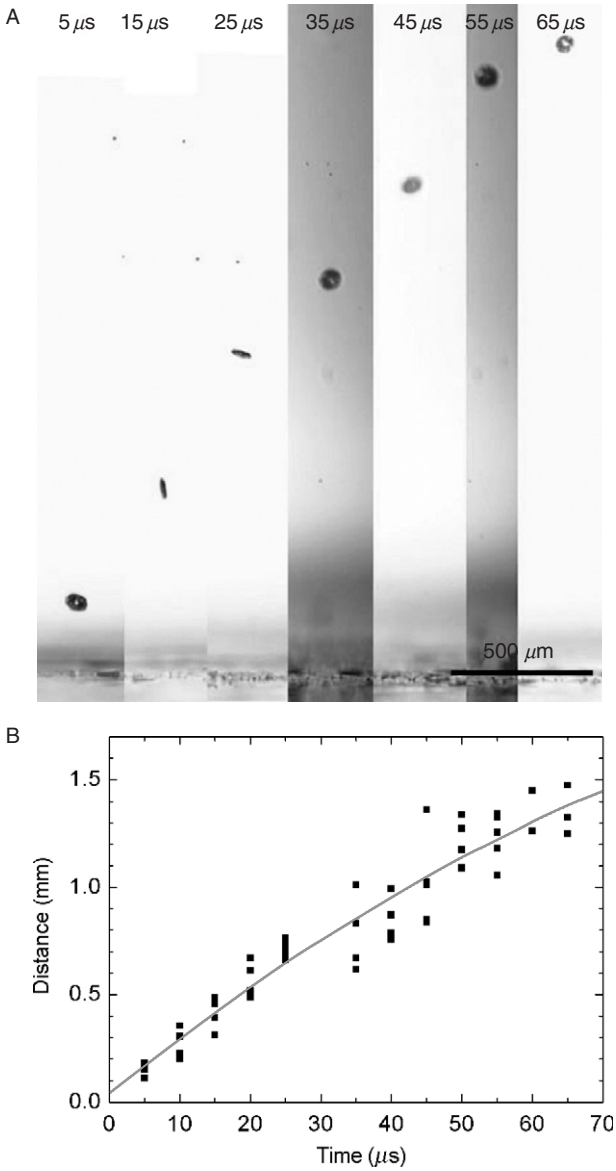

Fig. 11 Slowing of the specimens due to the friction in air. (A) shows a pictorial representation of the flight trajectory during the first 65 μs that is compiled of individual images taken at different delay times and (B) shows all measurement data on the flight distance versus delay time. The specimens had 80-μm diameter and were catapulted using a 40×, NA = 0.6 objective, and E = 6.5 μJ. The fitted curve corresponds to Eq. (4).

$$z(t) = K^{-1}\ln[kv_0(t - t_0) + 1] \quad (4)$$

where v_0 is the initial velocity at time t_0 denoting the duration of the acceleration phase, and K is a constant incorporating all material parameters including its density, cross-sectional area, and shape-related properties. Equation (4) was fitted to the measurement points in Figs. 8B, C, and 11B to obtain information on v_0 and t_0. Generally, good agreement between the trend exhibited by the experimental data and the fitted $z(t)$ curves was found. At later times >1 ms, when the specimen velocities have slowed down to ≤ 1 m/s, the hydrodynamic drag must be described by a combination of Newtonian friction ($\propto v^2$) and Stokes friction ($\propto v$), which leads to a more complex equation of motion (Elvers *et al.*, 2005).

In the experiments described above, the catapulting laser pulse was aimed at the center of the specimen to create optimum reproducibility. By contrast, in commercial microbeam systems, the region of interest is usually dissected in such a way that a small bridge is left at the location where the end of the trajectory of the cut would meet the starting point. A single pulse of larger energy is then aimed at the bridge in order to complete dissection and, at the same time, catapult the specimen. This strategy saves processing time but due to the reduced confinement of ablation products, the impulse coupling to the specimen is not as good as with laser pulses aimed at the center of the specimen. To optimize impulse coupling to the specimen, the width of the bridge should be at least equal to the diameter of the laser spot, and the spot size should be as large as possible without compromising the dissection of the bridge at the given pulse energy (Elvers *et al.*, 2005).

Another problem arising when the catapulting pulses are aimed at the rim of the specimen is that the flight trajectories are generally not in line with the optical axis of the microscope but oblique, as shown in Fig. 12. As a consequence, not all catapulted specimens arrive in the cap of the microfuge tube. In our investigations, about 93% of all dissectats would have arrived within the cap, and 65% would have reached its top part where the chance of adhesion is largest. The oblique direction of the flight trajectories is related to the fact that plasma formation at the rim of the specimen imparts an impulse not only in upward but also in lateral direction. Additionally, it causes a fast rotational movement of the specimen as visible in Fig. 13. The initial rotation frequency deduced from Fig. 13 is 500,000 rps, but it will probably vary from shot to shot. The rotation of a moving object induces a lateral force (Magnus effect) that will add to the lateral impulse imparted by the initial plasma expansion.

3. Catapulting with Defocused Pulses

To identify the gentlest way of catapulting, we investigated how the catapulting behavior depends on the size of the irradiated spot at the bottom of the specimen. The dependence of the initial velocities of the specimen and of the ejected particulate debris on spot size is presented in Fig. 14A and B. These graphs contain only a few data points because it is very time consuming to determine the initial velocity

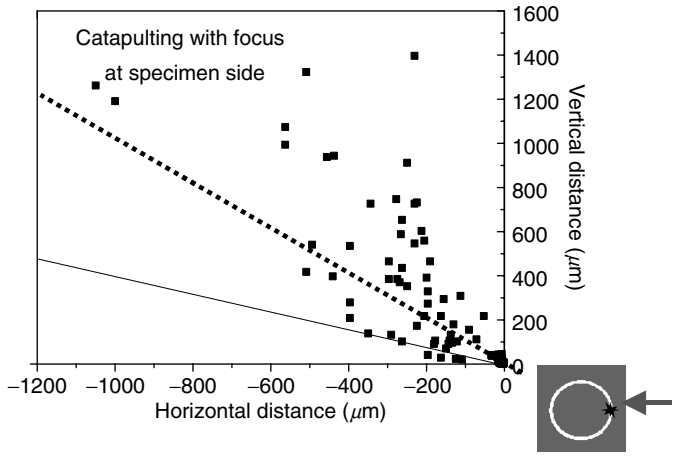

Fig. 12 Directional distribution of flight directions when the laser pulses are aimed at the rim of the specimen. Specimen diameter 80 μm, 40× objective, NA = 0.6, and E = 5 μJ. The specimens were photographed at different times after the catapulting laser pulse, and the data points show their location at these times. The flight trajectories are given by the connection between the laser focus (at 0,0) and the respective data points. The straight line delineates which specimen will reach the cap of the microfuge tube if it is located at a distance of 1 mm from the supporting slide and if the center of the cap is in line with the optical axis of the microscope objective. The dashed line indicates which specimens would reach the top of the cap, which is commonly wetted by a drop of mineral oil to improve adhesion.

values by taking series of images at different time delays as shown in Figs. 6 and 7. To cover a larger range of spot sizes, we took images at one delay time (50 μs after the laser pulse) and determined the average velocity during this flight time as shown in Fig. 14C. It is obvious that the catapulting velocities first increase and then decrease when the irradiated spot is enlarged. To facilitate the analysis of the underlying mechanistic changes, we inspected some catapulted specimens by scanning electron microscopy (SEM). The results are shown in Fig. 15.

Catapulting with tightly focused laser pulses is always associated with plasma formation and the generation of a hole through the entire specimen (Fig. 15A). With moderate defocusing, plasma formation is replaced by explosive vaporization, resulting in hole formation in the polymer foil but not in the specimen, with a zone around the hole where the foil melts and resolidifies (Fig. 15B). In this regime, the catapulting velocities are maximal (Fig. 14) because the ablation products remain confined below the specimen and cannot escape through a hole in the center of the specimen. More strongly defocused laser pulses lead to local ablation and melting of the foil, but do not perforate it (Fig. 15C). Pointlike ablated spots, but without obvious signs of surrounding melting, are also observed when the irradiated spot becomes comparable to or larger than the specimen size (Fig. 15D). In this regime, catapulting occurs still in a reproducible fashion but the velocities are much smaller than with focused and moderately defocused pulses (Fig. 14).

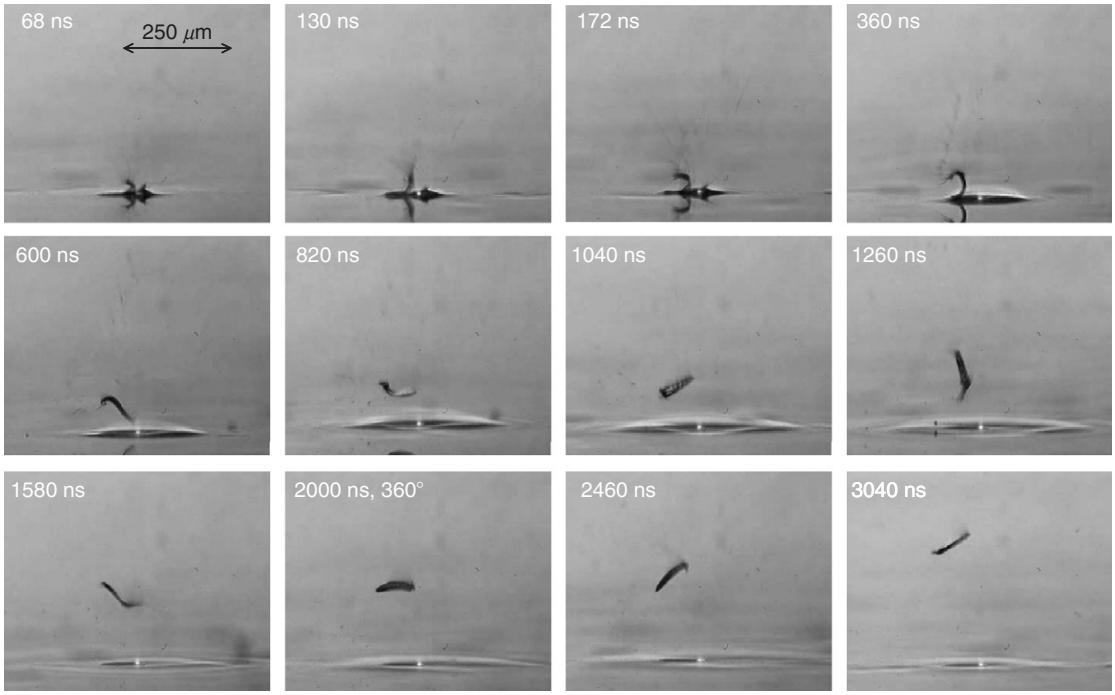

Fig. 13 Dynamics of a PEN foil specimen with 100-μm diameter that was first completely dissected and then catapulted by a 20-μJ pulse focused through a 20× objective and NA = 0.5 onto the rim of the specimen. The specimen performs one revolution within 2 μs, corresponding to a frequency of 500,000 rps.

For further analysis of the mechanisms of defocused catapulting, we calculated the average temperature rise within the irradiated spot in a layer with the thickness of the optical penetration depth, assuming a homogeneous light distribution in the irradiated spot. The calculation was based on the measured optical and thermal properties (heat capacity) listed in Table I. Because of the pronounced scattering of the PEN foil, 22.4% of the incident light are backscattered. This has been considered in calculating the temperature rise in the PEN foil, as well as the slight transmission loss pf 5.3% in the microscope glass slide. The results for the average laser-induced temperature in a PEN layer with the thickness of the optical penetration depth (0.88 μm) are presented in Fig. 16. The threshold radiant exposures for catapulting determined with different microscope objectives and laser pulse energies are listed in Table II, together with the corresponding temperatures of the light-absorbing layer. The thresholds were determined with strongly defocused laser beams, that is, in a catapulting mode for which hole formation in the specimen can be excluded.

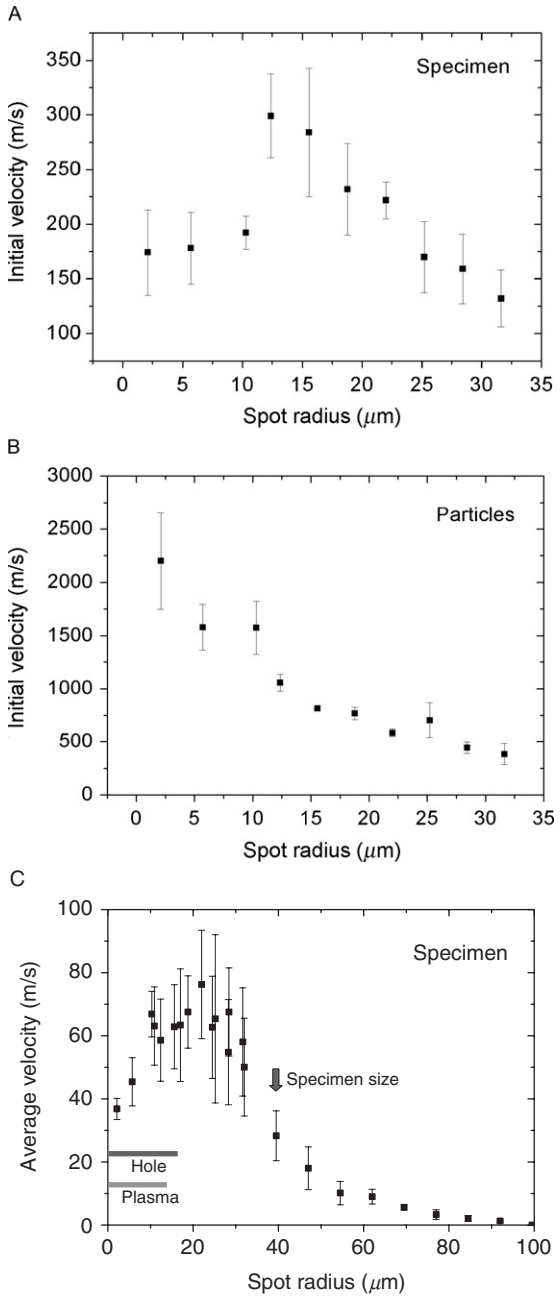

Fig. 14 Catapulting velocity as a function of laser spot size. (A) Initial velocity of the specimens, (B) initial velocity of the particulate debris, and (C) average velocity of the specimens during the first 50-μs flight time, with regimes for plasma and hole formation. 40× objective, NA = 0.6, and E = 10 μJ. The center of the irradiated spot coincided with the center of the specimen.

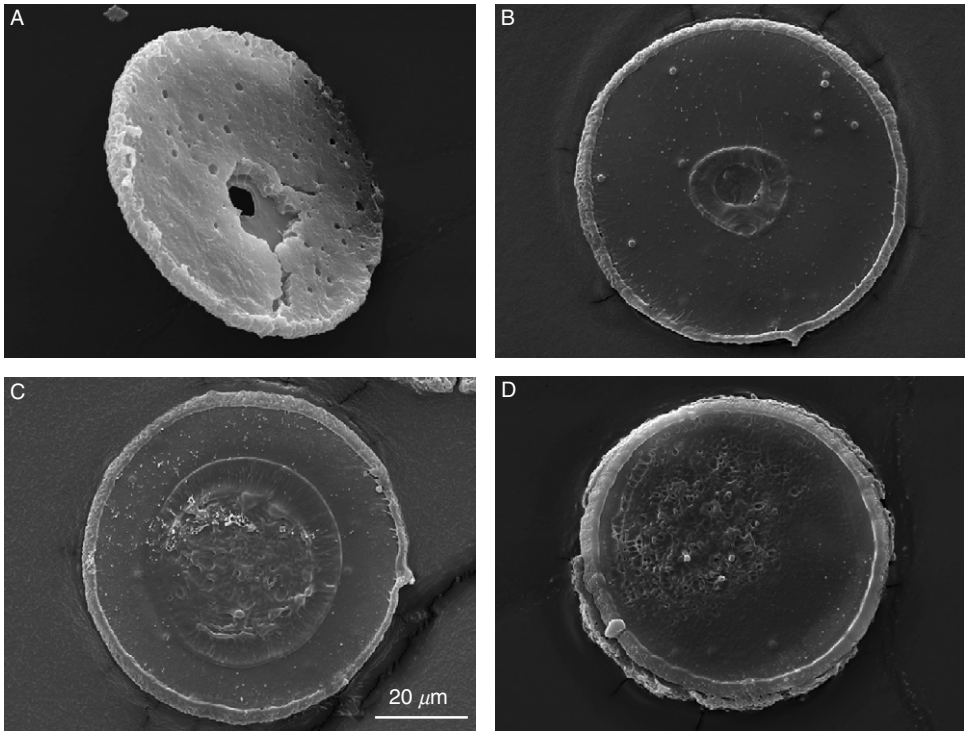

Fig. 15 Scanning electron micrographs of histologic specimens that were catapulted with irradiation of different spot sizes. The spot diameter is (A) 4, (B) 15, (C) 80, and (D) 136 μm. These values denote the diameter of the geometric cone angle of the laser beam at the location of the specimen. The actual spot size may be smaller if the irradiance distribution has an intensity peak around the optical axis.

The calculated peak temperatures for tightly focused irradiation ($\approx 10^5$ K) are unrealistically large because the calculation does not consider that the plasma expansion and adiabatic cooling already start during the laser pulse. Realistic plasma temperatures are in the order of 5000–10,000 K (Stolarski *et al.*, 1995). With defocused irradiation, for which catapulting is driven by ablation without plasma formation, adiabatic cooling by the expansion of the ablation plume reaches a significant level only toward the end of the laser pulse when most of the laser energy has been deposited (Apitz and Vogel, 2005). Therefore, the calculated peak temperatures at the bottom of the specimen are realistic. The calculated temperature rise for the spot radius of 22 μm associated with the maximum catapulting velocity is $\sim$1400°C. This is considerably larger than the melting temperature of PEN (269°C for slow heating, see Fig. 4), and also larger than the dissociation temperature (462°C for slow heating, see Table I). At the same time, it is lower than typical plasma temperatures, which is consistent with the fact that no plasma luminescence was observed. A temperature jump of 1400°C within 3 ns will be associated with explosive

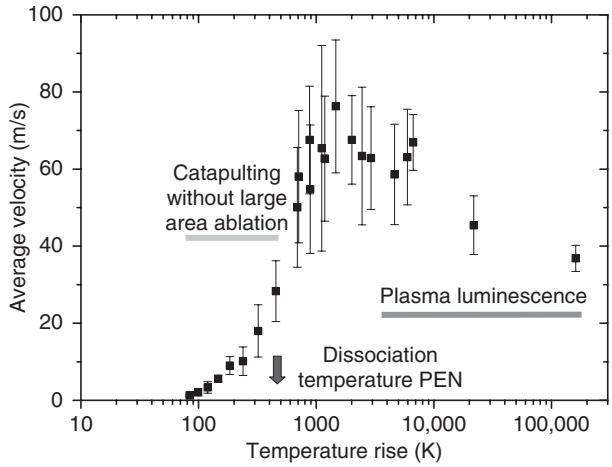

Fig. 16 Velocity data of Fig. 14C plotted as a function of the temperature rise at the bottom of the specimen. The average temperature rise in the optically absorbing layer is calculated based on the laser pulse energy (10 μJ), the measured optical penetration depth (0.88 μm), and an average value of the heat capacity of the PEN foil (2.7 J/g K, see Fig. 3). Losses by specular reflection at the glass slide, absorption in the glass (together 5.3%), and by backscattering from the PEN foil (22.4%) were taken into account.

Table II
Catapulting Thresholds for 3-ns, 337-nm Irradiation

	40× objective			5× objective		
Energy (μJ)	ΔT (K)	ϕ_{th} (J/cm^2)	I_{th} (MW/cm^2)	ΔT (K)	ϕ_{th} (J/cm^2)	I_{th} (MW/cm^2)
10	50	0.03	10	120	0.07	23.3
5	100	0.09	30	200	0.15	50

dissociation of the heated PEN material followed by a very rapid volume expansion. This is a very efficient catapulting mechanism (Fabbro *et al.*, 1990).

Interestingly, the specimens can still be catapulted when the average temperature rise in the absorbing layer is less than one-quarter of the dissociation temperature of the PEN foil. The observation that average temperatures well below the dissociation limit are sufficient for catapulting may indicate that the specimen is driven by sudden thermal expansion and deformation [similar to the working mechanism of dry laser cleaning (Luk'yanchuk, 2002; Tam *et al.*, 1992)]. Even though the actual surface movement caused by thermal expansion is very small, this expansion is achieved in the laser pulse duration of a few nanoseconds. Therefore, the acceleration by 1D surface expansion is 10^5–10^7 times larger than gravitational acceleration, leading to velocities in the order of 1 m/s at the end of

the laser pulse (Arnold, 2002; Tam *et al.*, 1992). Moreover, because of the small size of the specimen, thermal expansion can also occur in lateral direction. It is stronger in the lower part of the specimen where higher temperatures are reached than the upper part. This difference results in an upward bending of the peripheral parts of the dissectat that probably contributes to its upward acceleration. However, it is unlikely that these effects alone can account for specimen velocities of up to 20 m/s that were observed with irradiation parameters for which the average temperature in the absorbing layer is below the dissection threshold. We need to consider that the beam profile of the N_2 laser is highly irregular (Fig. 3B and C), that the temperature at the irradiated specimen surface is larger than the average temperature within the optical penetration depth shown in Fig. 16, that the SEM picture in Fig. 15D) is indicative for scattered pointlike ablation, and that the volume expansion of ablated material in confined geometry is an extremely efficient catapulting mechanism (Fabbro *et al.*, 1990). Thus even when the specimen's acceleration by thermal deformation becomes relevant, it is probably still accompanied by the propelling action of ablation in hot spots of the laser beam.

While for focused beams the catapulting velocities are larger when a 5× objective is used instead of a 40× objective (see Section III.B.1), we found no significant difference between the velocities achieved at a given energy when the irradiated spot is sufficiently large to exclude hole formation in the specimen for both objectives. The threshold radiant exposure for catapulting is even slightly lower for the 40× objective (see Table II). It is important to note that the degree of defocusing required to exclude hole formation increases when lasers with better beam quality (i.e., smaller focal spot size) than the N_2 laser are used.

We conclude that catapulting with defocused pulses relies on the pressure produced by confined ablation and, for large spots, possibly also on thermal expansion and deformation of the dissectat. The relative contributions of ablation and thermoelastic forces need to be further investigated.

C. Possible Side Effects and Their Minimization

1. Thermal Effects

The high temperatures produced during plasma formation or pulsed laser ablation seem to be an obvious source for potential side effects of LMD and LPC. However, one needs to consider that any changes within the material that is disintegrated or vaporized during the cutting process do not affect the accuracy of the subsequent genomic or proteomic analysis. Of interest are only changes by heat conduction or convection which alter the remaining dissected specimen that is catapulted into the cap of the microfuge tube.

Let us first consider LMD and LPC with *tightly focused laser pulses*: Here the fraction of the specimen exposed to high temperatures is very small, and most of it is disintegrated and does not take part in the subsequent analysis. Because of the fast adiabatic cooling during the rapid expansion of the laser-induced plasma, the time

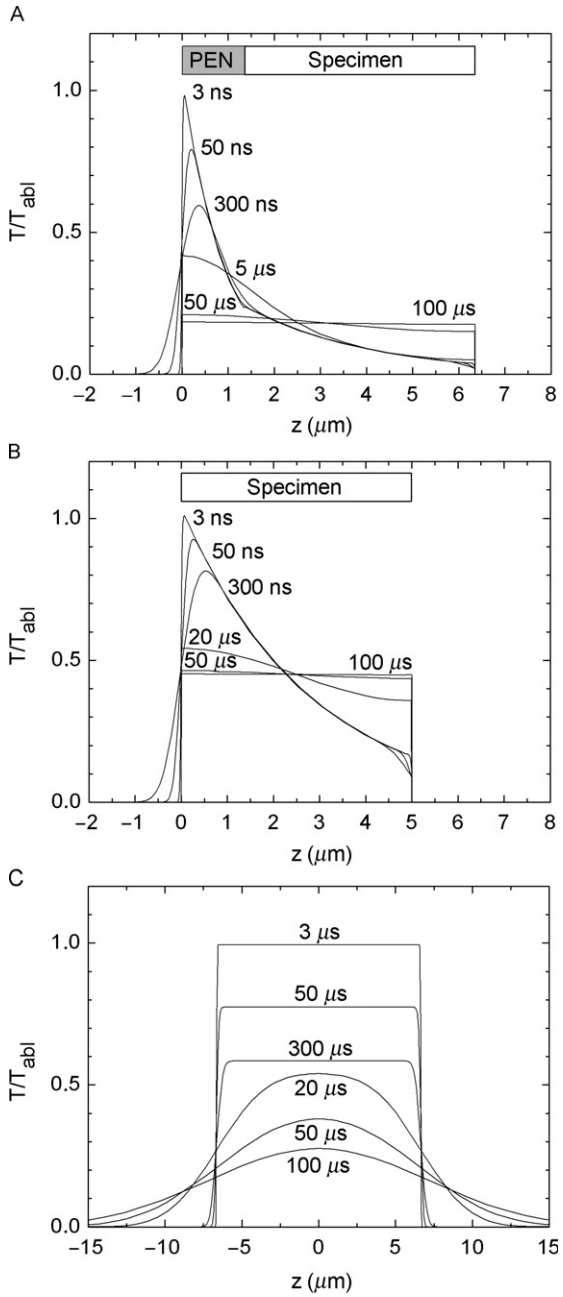

Fig. 17 Evolution of the temperature distribution for (A) H&E-stained specimen on PEN foil backed by a glass slide, homogeneously irradiated by a defocused laser pulse; (B) H&E-stained specimen on a glass slide, homogeneously irradiated by a defocused laser pulse; and (C) H&E-stained specimen on a

available for heat conduction into adjacent parts of the specimen is extremely short (<1 μs), and the heat-affected zone next to a cut is therefore very small. The width of the altered region at the rim of the dissectat in the SEM pictures of Fig. 15 amounts to 2–3 μm for the bottom side covered with PEN foil (Fig. 15B–D) but is smaller (<1 μm) for the upper side, that is for the histologic specimen itself. The fact that thermal alterations are most pronounced at the bottom side of the dissectat can be attributed to heat diffusion from the plasma through the supporting glass slide, which is a good heat conductor. The small amount of thermal damage in the histologic specimen is consistent with previous transmission electron microscopical studies of plasma-mediated dissections in ocular tissues performed with IR laser pulses of 6-ns and 40-ps duration in which the heat affected zone was found to be far below 1 μm (Niemz *et al.*, 1991; Vogel *et al.*, 1990).

The situation is less obvious when a larger fraction of the specimen is exposed to the laser radiation, that is, for moderate or strong defocusing, and when the sample is catapulted directly from a glass slide, without protection by the light-absorbing PEN foil. To assess potential side effects by thermal damage for these cases, we calculated the time evolution of the temperature distribution under different focusing conditions of the laser pulse, as shown in Fig. 17.

We used an analytical solution of the differential equations for heat diffusion in a multilayer geometry (Freund *et al.*, 1996), with layers representing glass, PEN foil, histologic specimen, and air. Glass and air were supposed to be transparent, and the absorption properties of PEN foil and histologic section were assumed to be in accordance with Lambert-Beer's law and taken from Table I. Calculations were performed for a laser pulse with rectangular temporal shape and 3-ns duration. As analytical solutions for layered geometries with different optical properties are restricted to homogeneous thermal properties of the medium, we had to use the same values for heat capacity, heat conductivity, and mass density for all layers. We employed the measured data for haematoxylin and eosin (H&E)-stained specimens listed in Table I.

We assumed that heat can diffuse from the light-absorbing PEN foil and histologic section into the adjacent glass slide until the specimen detaches from the slide during the expansion of the ablation plume, which occurs about 300 ns after the laser pulse (Fig. 6). Afterward, the calculations were continued for a thermally isolated specimen because heat conduction into the surrounding air is negligible. The adiabatic conditions were simulated by the introduction of appropriate mirror heat sources (Carslaw and Jaeger, 1959).

For catapulting without plasma formation, the temperature of the sample surface is determined by the ablation temperature T_{abl} of the sample material. For polymers, the ablation temperature corresponds to the dissociation temperatures

glass slide, irradiated by a pulse with top-hat distribution of 15-μm diameter. The plots in (A) and (B) show the temperature distribution in z-direction; the distribution in lateral direction is homogeneous. The plots in (C) present the lateral temperature distribution at the surface of the heated localized area; the temperature decay in z-direction resembles that in (B) and is not shown.

that, for slow heating, are given in Table I. At very short heat exposure times, dissociation temperatures are higher because dissociation is a chemical rate process (Pearce and Thomsen, 1995). In a similar way, the temperature required for protein denaturation increases with decreasing heat exposure time (Huttman and Birngruber, 1999; Pearce and Thomsen, 1995; Simanowski *et al*., 2005). This rise of dissociation and denaturation temperatures could not be considered in our calculations because the rate constants for very fast heating are not yet known. To avoid this difficulty, all temperatures in Fig. 17 are not given in absolute values but normalized to the maximum temperature at the sample surface reached at the end of the laser pulse.

Figure 17 compares the temperature evolution for cases where an H&E-stained specimen is either mounted on PEN foil backed by a glass slide (Fig. 17A) or directly placed on the glass slide (Fig. 17B). In both cases the samples were homogeneously irradiated by a *strongly defocused laser beam*, and the temperature distribution in lateral direction is thus also homogenous. When the histologic specimen is mounted on PEN foil, the ablation temperature is reached at the glass–PEN interface, and the specimen itself is well protected by the strong laser light attenuation in the PEN material. The equilibrium temperature reached 50–100 μs after the end of the laser pulse amounts to only 20% of the ablation temperature, and even at the PEN-specimen interface the temperature never exceeds 35% of the PEN ablation temperature (Fig. 17A). By contrast, when the specimen is placed directly on glass, the specimen's ablation temperature (which is lower than for PEN, see Table I) must be reached at the surface of the specimen itself. Moreover, since the laser light penetrates deeper into the specimen material than into PEN, the initial temperature distribution in Fig. 17B is broader than in Fig. 17A, and the equilibrium temperature reached 50–100 μs after catapulting is higher; it amounts to 45% of the ablation temperature. Catapulting directly from glass with spatially homogeneous irradiation thus should be avoided if possible. The thermal load from tightly focused laser irradiation is much smaller, as discussed in the beginning of this section, but the amount of material transported per pulse will also be smaller than with homogeneous irradiation if no PEN foil is used.

The modeling results of Fig. 17A predicting that the histologic specimen on top of the 1.35-μm-thick PEN foil is hardly affected by heat are in good agreement with the SEM results of Fig. 15D for strongly defocused catapulting which demonstrate that only the bottom of the polymer foil is ablated. However, even when PEN foil is used, the specimen is not in all cases protected. The SEM images in Fig. 15B show that with *moderate defocusing* corresponding to 15-μm spot diameter the PEN foil is removed from the irradiated area. A part of the PEN material has probably been ablated and another part was molten and pushed aside by the pressure in the ablation cloud. Therefore, the lower surface of the histologic specimen is exposed to the PEN ablation temperature, and the temperature profiles in z-direction will thus resemble those of Fig. 17B. However, because of the small size of the irradiated spot, lateral heat diffusion now contributes to cooling as shown in Fig. 17C, and the cooling continues even after the specimen is

thermally isolated form the glass slide. As a consequence, the temperature at the specimen surface drops to 28% of the ablation temperature within 100 μs, compared to 45% in Fig. 17B. Nevertheless, with moderate defocusing it cannot be excluded that the nonablated specimen volume above the perforated area and next to the molten foil is subject to thermal changes. However, for a spot diameter of 15 μm and a specimen diameter of 80 μm, this volume corresponds to only 3% of the entire specimen volume. For 25-μm spot size, the fraction increases to 10%.

2. Photodamage by UV Light

Chemical changes by UV light are, like thermal damage, only relevant for the material remaining after dissection. During dissection and catapulting with focused laser pulses, the dissectat may be irradiated by UV laser light scattered at the laser plasma and by the UV plasma luminescence. The light scattering by ns plasmas was found to involve less than 2% of the incident laser irradiation and to occur mainly in forward and backward direction (Nahen and Vogel, 1996). Therefore, the scattered laser light may, at worst, affect a very thin specimen layer at the edge of the cut that is of little relevance for LMD and LPC. The energy of the plasma radiation stays below 0.1% of the incident laser energy (Vogel *et al.*, 1999) and is thus completely irrelevant.

During defocused catapulting with an extended spot size, a large fraction of the specimen or the entire specimen is exposed to the laser light. However, the histologic section is protected by the PEN polymer foil that transmits only 20.5% of the incident light at 337 nm (Table I). Furthermore, the N_2 laser wavelength of 337 nm is far away from the peak of the action spectrum for DNA damage shown in Fig. 18 (Coohill, 2002), and the wavelength of a frequency-tripled Nd:YAG laser (355 nm) is even further away. This is consistent with investigations on the wavelength dependence of laser-induced DNA damage in lymphocytes using the comet assay (de With and Greulich, 1995). For $\lambda = 340$ nm, the detection threshold for DNA damage found by de With and Greulich (1995) corresponded to a radiant exposure of 1.5 J/cm^2. Because of the limited sensitivity of the comet assay, $\sim$300 strand breaks per cell are necessary to detect DNA damage. Hence, one single DNA strand break per cell is expected to occur after a radiant exposure of 5 mJ/cm^2. Other pathways of cell damage in the UV-A/B region of the optical spectrum involve the generation of reactive oxygen species such as H_2O_2 and OH* radical (Bertling *et al.*, 1996; Hockberger *et al.*, 1999; Tyrrell and Keyse, 1990). For broadband radiation (305–350 nm) peaking at 325 nm, significant cell killing was observed with light doses $\geq$1 J/cm^2 (Bertling *et al.*, 1996).

The total dose arriving at the PEN foil when a 10-μJ pulse irradiates a specimen with 80-μm diameter is 200 mJ/cm^2. The dose transmitted through the foil and arriving at the histologic material is 40 mJ/cm^2. This is 25 times below the threshold for cell killing reported by Bertling *et al.* (1996), but slightly above the dose causing, on average, one DNA single strand break per cell (de With and Greulich, 1995).

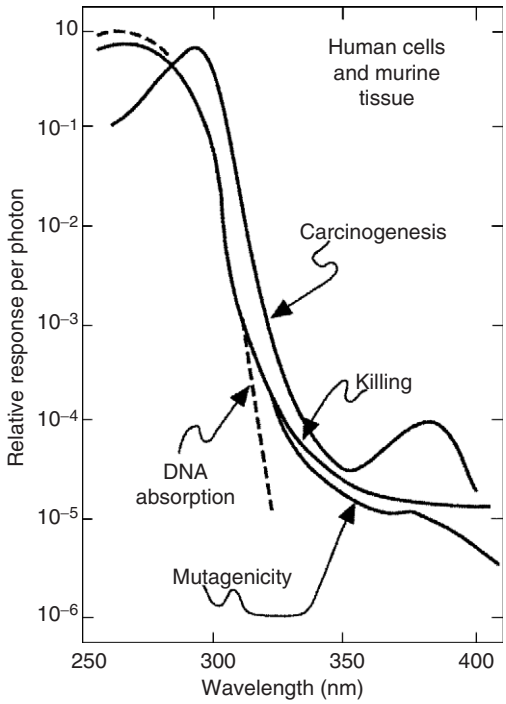

Fig. 18 UV action spectra for human cell killing, mutagenicity, DNA strand breaks, and DNA-protein cross-links. Reprinted with permission from Coohill (2002). Copyright CRC Press.

With moderate defocusing, for example for 15 μm spot diameter, the dose within the irradiated area increases by a factor of 30 to 6 mJ/cm^2, and the protection by the PEN foil is largely absent because it is ablated by the catapulting laser pulse (Fig. 15B). In this case, the risk for UV damage directly above the irradiated spot is higher because the radiant exposure exceeds the value of 1 J/cm^2 leading to significant cell damage, and largely exceeds the threshold value of 5 mJ/cm^2 for sporadic DNA strand breaks in individual cells. It is important to note, however, that for a specimen with 80-μm diameter, only 3% of the total volume will be affected by the UV irradiation of a spot with 15-μm diameter. The affected fraction is larger when histologic material is directly catapulted from glass substrates without supporting polymer foils because in this case smaller amounts of material are catapulted per pulse.

3. Mechanical Deformation and Rupture

In general, purely mechanical rupture and disintegration of a histologic sample during LPC impose no problem for subsequent genomic or proteomic analysis because only a very small fraction of the biomolecules will be affected even if the

dissectat is fragmented into many large pieces. However, mechanical forces may affect the viability of live cells (see Section IV).

The specimen is accelerated to a speed of 180–350 m/s within about 200 ns (Fig. 14A). The acceleration in the initial phase of catapulting is thus enormous, being $\sim 10^8$ times larger than the gravitational acceleration. However, this does not affect the specimen's integrity as long as the accelerating forces are homogeneous because only tensile stress and shear forces lead to deformation and tearing.

The main sources of shear forces are pressure gradients, while tensile stresses may also originate from radial expansion movements (Lokhandwalla and Sturtevant, 2001; Lokhandwalla *et al.*, 2001). During focused LPC, the huge pressure gradients produced in the vicinity of the plasma lead to local rupture of the specimen, and the large absolute pressure values in this region result in the immediate ejection of debris at very high velocity. However, once the plasma pressure is partly released through the hole in the center of the specimen, the distribution of the driving forces becomes more homogeneous as the shock wave spreads laterally below the entire specimen. At this stage, the pressure gradients have become too small to cause further rupture or strong deformations, and the dissectat flies off in a disklike shape (Fig. 6).

More significant deformations may arise from moderately defocused laser pulses that do not produce a hole in the specimen. Because the irradiance is largest in the center of the irradiated spot (Fig. 3), the initial pressure distribution is inhomogeneous and the center of the specimen will bulge upward before it flies off. Such deformation can be avoided by creating a nearly homogeneous irradiance distribution across the specimen. This is possible by defocusing of the laser beam to a degree that the irradiated spot is much larger than the specimen, but that would be associated with considerable energy loss. Alternatively, a phase mask can be used to create a homogeneously illuminated spot with appropriate size.

4. Quantification of the Influence of Side Effects on the Accuracy of Proteomic and Genomic Analysis

LMD was originally developed to facilitate the histochemical analysis of cryosections (Meier-Ruge *et al.*, 1976). Correspondingly, the authors performed enzyme-histotopochemical investigations on N_2 laser dissected fragments of tissue sections to assess the quality of the procurement method. They observed a decrease of enzyme activity by 10–20% in a several microns thick region bordering the cut when dissection was performed at an energy level four times larger than that sufficient for cutting. The changes were attributed to heat diffusion from the glass support and characterized as not relevant for subsequent histochemical analysis.

At present, LMD is mostly combined with molecular biological analysis, including polymerase chain reaction (PCR) and microarrays for genomic and mass-spectrometry for proteomic studies. In qualitative and quantitative analysis of gene expression, reverse transcriptase PCR (RT-PCR) plays a prominent role. In principle, the method allows very small numbers of molecules to be detected

at extreme sensitivity and high specificity (Bustin, 2000), and is therefore the preferred method for the analysis of tiny tissue fragments procured in LMD and LPC. Initially, Schütze and Lahr (1998) used formalin-fixed and paraffin-embedded tissue sections supported by a PEN foil, isolated tissue fragments by LMD and LPC, and successfully detected specific mRNA sequences in RT-PCR. Since then, it is known that numerous factors, including fixation, tissue processing, staining and labeling, and probably also laser dissection may reduce the content of mRNA in the tissue samples by several orders of magnitude and thus may critically affect quantitative analyses (von Smolinski *et al.*, 2005, 2006). A major effect on the mRNA loss can be attributed to chemical fixation in aldehydes and embedding in paraffin, as typically done in histopathology (Krafft *et al.*, 1997; Lewis *et al.*, 2001; Stanta and Schneider, 1991). As compared to unfixed cryosections, this classical tissue processing reduces the mRNA by factors of 85–99% (Abrahamsen *et al.*, 2003; von Smolinski *et al.*, 2005). In addition, conventional staining protocols (e.g., H&E) or immunohistochemical labeling (e.g., for fluorescence microscopy) also attribute to mRNA loss by factors of up to 99.8% (von Smolinski *et al.*, 2006). It must be assumed that thermal effects and those evoked by UV light during LMD and LPC can produce some additional damage to the mRNA contained in the isolated samples, but quantitative data on the absolute mRNA loss and on the relative loss compared to the factors mentioned above are still lacking. In this context, it should be noted that mechanical damage occurring during LPC of histologic specimens would not affect the accuracy of protein or gene analysis (Schütze and Lahr, 1998) because crushing of the samples is a prerequisite for many analytical techniques in biochemistry and molecular biology. In contrast, the extent of thermal and UV light damage will depend on the size of individual dissected section fragments, which vary in area between some hundred square microns for single cells and several 10,000 μm^2 for extended tissue compartments isolated in tumor biology or immunological research. As discussed in Sections II.C.1 and III.C.2, only little collateral damage is produced when large specimens are catapulted with tightly focused or strongly defocused laser pulses. The influence of heat and UV radiation is largest with moderately defocused pulses.

Besides PCR analysis in genomics, the analysis of proteins is a further interesting and promising application for laser tissue microdissection. Tiny amounts of protein are analyzed using mass spectrometry (Ai *et al.*, 2006; Fink *et al.*, 2006) or microarray techniques (Gulmann *et al.*, 2005; Niyaz *et al.*, 2005). Using an antibody-ultramicroarray, proteins can be detected with high specificity and sensitivity amounts equaling less than 10 cells (Nettikadan *et al.*, 2006). A novel method is the so-called proteohistography which combines array- and mass-spectrometric techniques and produces an image of the spatial distribution of proteins in a given tissue area (Ernst *et al.*, 2006).

The maximum likelihood for laser-induced unwanted side effects in both proteomics and genomics arises when histologic material is directly catapulted from glass substrates without supporting polymer foils. In this case, the laser beam has

to be scanned across the area to be catapulted. The large number of applied pulses and the lack of a protecting polymer foil involve an increased exposure to both UV radiation and heat. Preliminary investigations revealed that mRNA recovery from cryosections decreases considerably if the material is catapulted from glass without the use of a PEN foil. To compare both methods, eight identical samples were processed both with PEN foil and without foil in the auto-LPC mode using factory settings of the instrument. The amount of intact mRNA copies of the housekeeping gene EF1α remaining in the sample after catapulting was determined using real-time PCR. After catapulting directly from glass, 35.5–40.00 amplification cycles were necessary to achieve a certain signal strength as compared to 26.1–28.2 cycles when a PEN foil was used (Dorthe von Smolinski, Institute of Anatomy, University of Lübeck, unpublished results). Since the amount of genetic material is doubled in each cycle, an increase by one cycle (1- Ct unit) corresponds to a loss of 50% specific mRNA in the sample, and an increase of 7- to 9-Ct units indicates a loss of 99.2–99.8% of specific mRNA copies. This value resembles the loss observed otherwise as a consequence of fixation, embedding, and staining. Our preliminary results thus indicate that there is still a large potential for improving laser-assisted mRNA recovery from cryosections. A systematic analysis of potential side effects of the different LMD and LPC procedures and of ways to optimize the accuracy of the genomic or proteomic analysis still needs to be performed.

IV. Dissection and Catapulting of Live Cells

For the retrieval of live cells by LMPC we used a protocol based on the use of duplex membrane dishes that was adopted from Mayer *et al.* (2002) and Stich *et al.* (2003). A 25-μm-thick Teflon membrane provides mechanical support, and a 1.35-μm-thick PEN foil conditioned with polylysine is mounted into the dish above the Teflon membrane as delineated in Fig. 19. CHO cells were cultivated on this foil until a confluent monolayer had developed. Before LMPC, the culture medium was almost completely removed such that only a thin layer of liquid (up to 40-μm thick, as determined by optical coherence tomography, OCT) remained above the cells. Then the region of interest was dissected, and the dissectat (cells and PEN foil) catapulted by a single laser pulse into the cap of a microfuge tube that had been wetted with culture medium. To test cell viability after LMPC, the cells were transferred into 12-well plates as described by Stich *et al.* (2003), and recultivated.

The original protocol involves the use of focused laser pulses for catapulting but we also performed series of experiments with defocused pulses because we hoped that this would minimize bending of the specimen and shear stresses on the cells. Some experiments were done without any fluid between Teflon membrane and PEN foil, but usually some liquid enters the space between the two membranes. Since we observed that the presence of this liquid has an influence on the catapulting

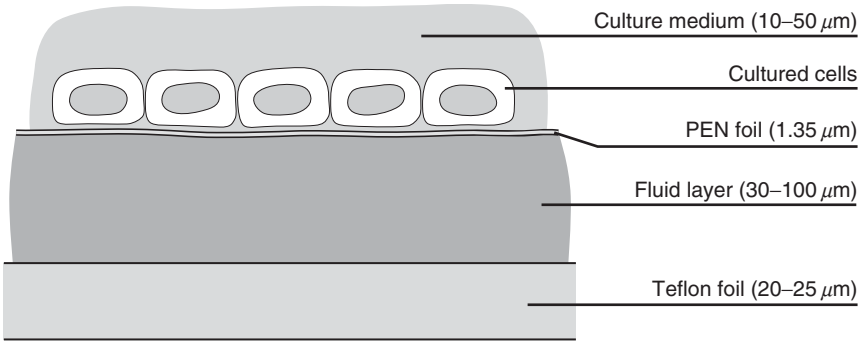

Fig. 19 Schematic presentation of the setup used for live-cell catapulting from a duplex membrane dish. Shortly before LMPC, the culture medium is almost completely removed such that only a thin layer of liquid remains above the cells.

dynamics, we performed additional experiments in which a well-defined amount of medium was injected between the membranes before LMPC. The resulting liquid layer had a thickness of 30–100 μm.

To document the dissection process before catapulting by time-resolved photography, we replaced the halogen lamp and collimation optics of the microscope by a Nanolite flash lamp combined with a Nikon 50 mm/1.2 objective used as collimator. Photographs of the dissection dynamics were taken through the microscope optics with single exposures at different time delays after the release of the dissecting laser pulse. The catapulting dynamics was photographed in side view using the setup described in Section III.B.1. To be able to photograph the initial catapulting phase without vignetting by the rim of the Petri dish, we developed a special dish with a removable rim. Teflon membrane and PEN foil were clamped around a stainless steel ring using a silicone O-ring. A flat silicone ring was placed on top of the steel ring. It was pinned down by the weight of a second stainless steel ring and thus provided a tight seal for the culture medium. After removal of most of the culture medium shortly before LMPC, the upper steel ring and the silicone seal could also be removed which offered an unobstructed view onto the cells on top of the PEN foil.

A. Dissection in a Liquid Environment

Even after removal of most of the culture medium, dissection takes place in a liquid environment. Thus the surrounding liquid confines the laser-produced plasma and the ablation products cannot freely escape. As a result, a transient cavitation bubble is formed around the laser focus (Venugopalan *et al.*, 2002; Vogel and Venugopalan, 2003, Chapter IX), which expands and collapses within a few microseconds. Because of the cavitation bubble dynamics, dissection in a liquid environment is less precise than in air. For sufficiently large laser pulse energies, the shear

stress exerted by the oscillating bubble causes lysis of cells adjacent to the laser focus (Rau *et al.*, 2004, 2006) or sweeps them off the PEN foil, if their adhesion is weak.

We observed that the energy required for dissection increases in the presence of a liquid layer between Teflon membrane and PEN foil, especially when this layer is thick (≈100 μm). Adhesion between cells and foil was observed to decrease when cells continued to grow after forming a confluent layer. Adhesion could be improved by conditioning the foil with polylysine. In Fig. 20A and B, cells are swept off the PEN foil by the expanding bubble up to a distance of 20–30 μm from the laser cut even though a pulse energy of not more than 1 μJ was used for dissection. The reason is that no polylysine had been applied, and the cell density on the foil was already fairly high indicating reduced adhesion. The bubble dynamics is presented in Fig. 20C and D. Here, a larger pulse energy of ≈6 μJ was required for dissection because the liquid layer between Teflon membrane and

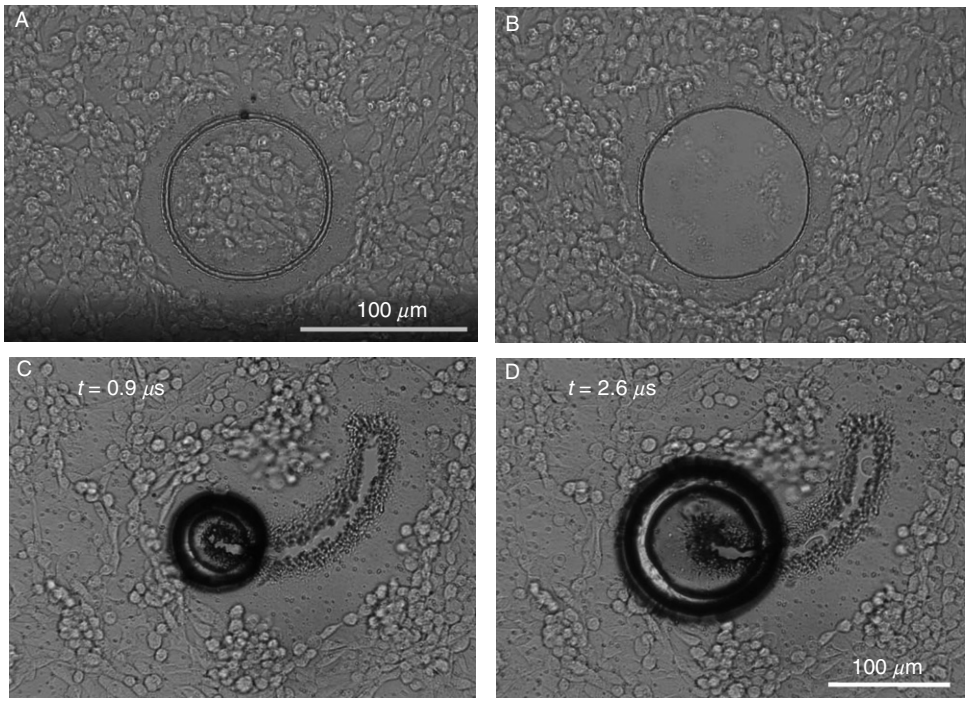

Fig. 20 Laser dissection and catapulting of CHO cells with relatively low adhesion to the PEN foil, (A) after dissection using a 20× objective, NA = 0.5, and E = 1.0 μJ, (B) after catapulting. The denudation near the cut is caused by the shear forces arising from the oscillating cavitation bubbles produced on optical breakdown in the culture medium. In (C) and (D) the cavitation bubble dynamics during dissection of CHO cells is shown at different times with (D) being the stage of maximum expansion. The dissection energy was here relatively large (E = 6 μJ) because the PEN foil was separated from the Teflon membrane below by an ≈100-μm-thick liquid layer.

PEN foil was fairly thick. The maximum bubble diameter amounts to ≈140 μm but the width of the denuded zone on the foil is smaller: it corresponds quite closely to the area in which the expanding bubble touches the cell layer. Under optimum conditions, the damage zone next to the cut amounts to about 5–8 μm, as shown in Fig. 21, which is considerably smaller than in Fig. 20.

We employed a 20× objective, NA = 0.5 both for dissection and catapulting, as described by Mayer *et al.* (2002) and Stich *et al.* (2003). Collateral damage during dissection can be reduced by using objectives with larger NA because they allow for plasma-mediated cutting with smaller pulse energies.

B. Catapulting of Live-Cell Populations

LMPC and recultivation of a colony of CHO cells is demonstrated in Fig. 21. To minimize the stress on the cells, we used small pulse energies for dissection and catapulting, and focused the catapulting pulse at the periphery of the specimen, as visible in Fig. 21C and D. The denuded zone at the sides of the cut is smaller than

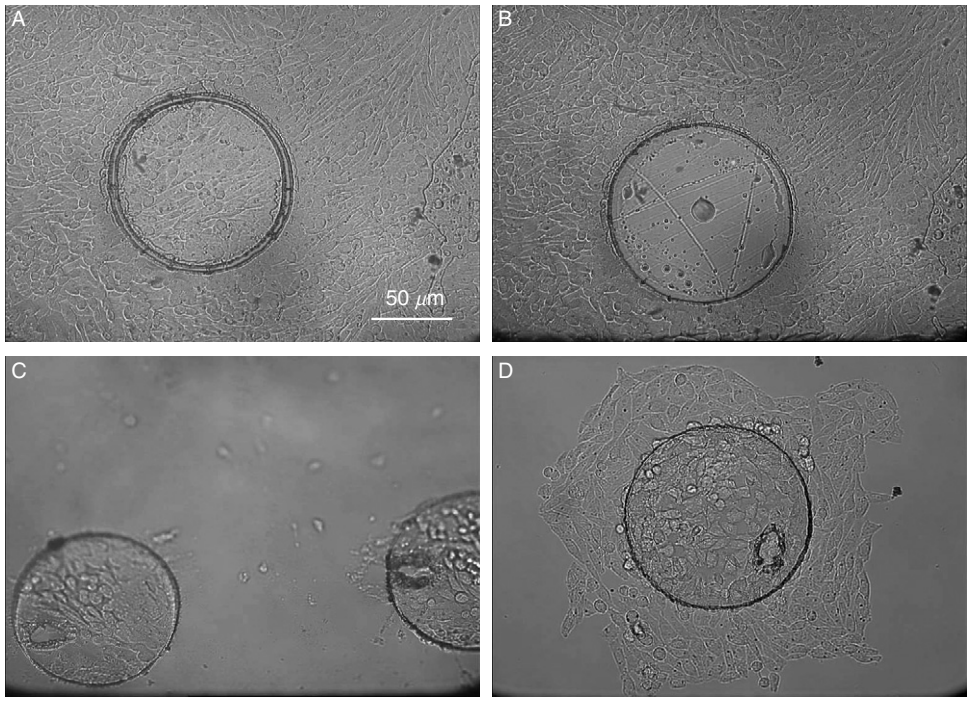

Fig. 21 Laser dissection, catapulting, and recultivation of a colony of CHO cells according to the protocol of Stich *et al.* (2003). (A) after dissection, (B) after catapulting with a focused pulse, (C) catapulted specimens in the cap of a microfuge tube, and (D) after 48 h of recultivation. We used a 20×, NA = 0.5 objective, with pulse energies of 1.0 μJ for dissection and 5.0 μJ for catapulting.

in Fig. 20 because the adhesion of the cells was better, and the liquid layer between Teflon membrane and PEN foil was thinner, which facilitates dissection.

When the laser pulse was focused into the periphery of the specimen, 16% of the catapulted specimens ($n = 60$) missed the cap for reasons already discussed in Section III.B.2. However, out of the specimens that could be transferred into a 12-well plate, 98% (all besides one) could be recultivated. Because we had observed that the use of a strongly defocused laser beam for catapulting of histologic specimens was associated with a stable flight trajectory, absence of hole formation, and moderate catapulting velocities (see Fig. 14), we tested this strategy also on live cells. We used the maximum defocusing setting on the microbeam station, corresponding to a spot diameter of 50 μm. As expected, all specimens (60 out of 60) arrived in the cap, but to our surprise the majority of the cells had been sheared off the foil, as shown in Fig. 22B and C. In only four cases (7%), recultivation was possible.

This puzzling difference is not easily understood, considering the complex geometry of membranes and liquid layers in live-cell catapulting (see Fig. 19). Therefore, we chose a stepwise approach to understand the role played by the individual layers. In the first series of experiments, a 30- to 50-μm-thick liquid layer was injected between Teflon membrane and PEN foil, but no cells or liquid was present on top of the foil. PEN dissectats of 100-μm diameter were catapulted with defocused laser pulses (50-μm spot diameter) and with pulses focused at the periphery of the specimen, and the resulting dynamics is shown in Fig. 23.

In defocused catapulting (Fig. 23A), the expanding ablation products drive the liquid below the specimen radially to the specimen's rim where it collides with the surrounding resting liquid. As a result, the liquid is pushed through the

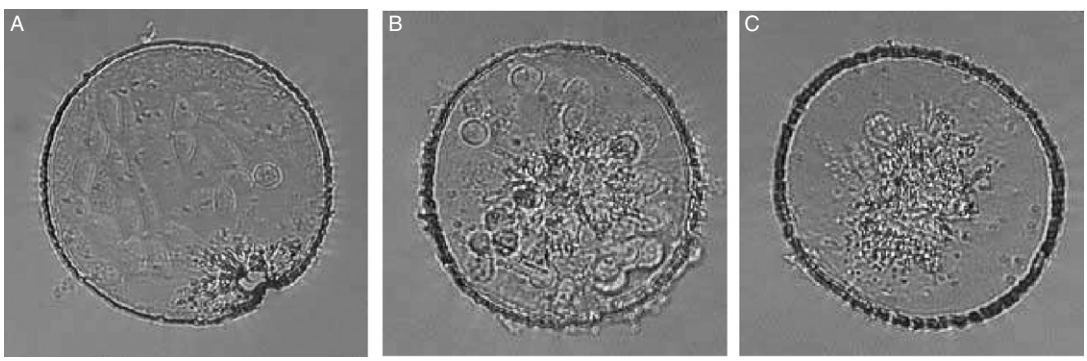

Fig. 22 Specimens after catapulting with focused (A) and moderately defocused laser pulses (B) and (C). In (A) all cells near the specimen center remained on the PEN foil but regions in the vicinity of the laser shot and at the opposite side of the specimen are denuded. In (B) some cells remained on the PEN foil, while the foil in (C) is completely denuded. The ablation pattern visible around the center of the specimen in (C) demonstrates that the intensity distribution in the catapulting laser beam is inhomogeneous.

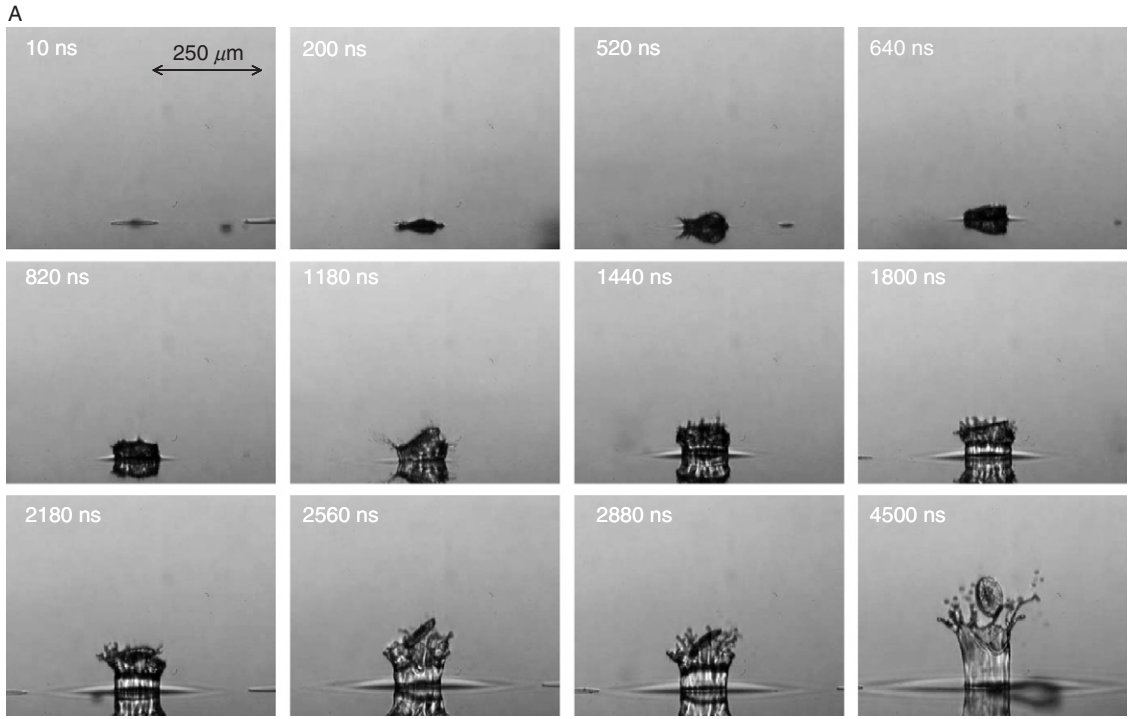
A
10 ns
250 μm
200 ns
520 ns
640 ns
820 ns
1180 ns
1440 ns
1800 ns
2180 ns
2560 ns
2880 ns
4500 ns

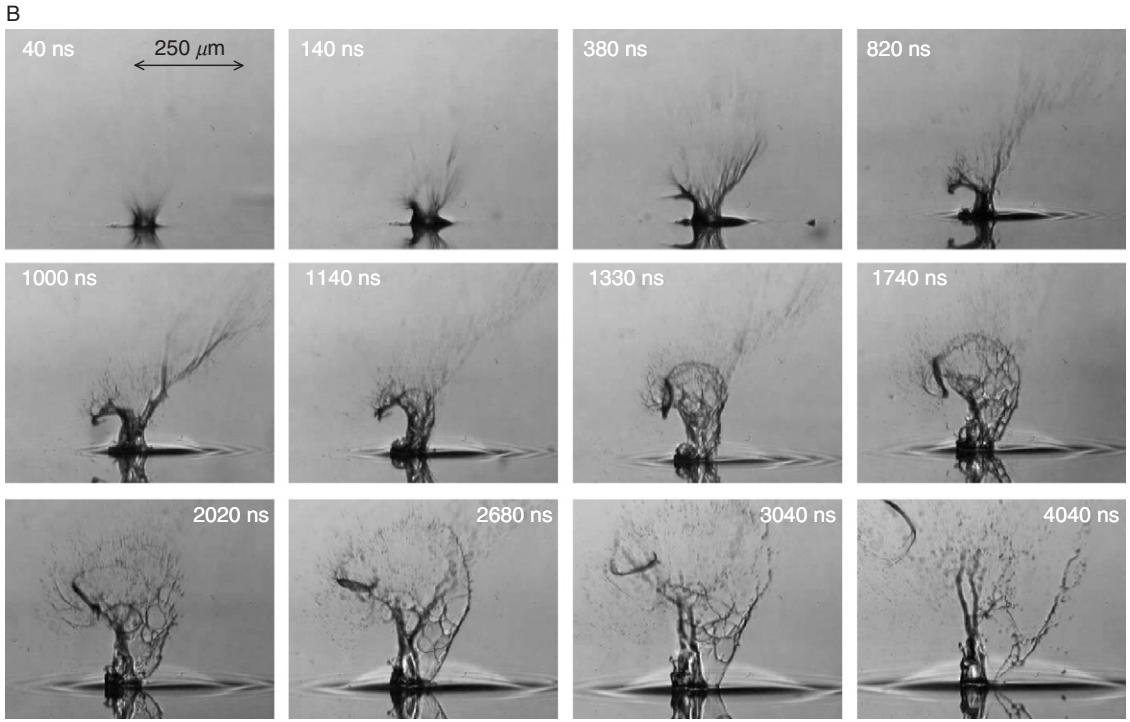

Fig. 23 Catapulting of PEN foil specimens located above a Teflon membrane, with a 30- to 50-μm-thick liquid layer between the two membranes. (A) Catapulting with defocused laser pulses aimed at the center of the specimen (50-μm spot diameter), (B) catapulting with pulses focused at the periphery of the specimen (the plasma luminescence indicates the location of the laser focus). 20$\times$ objective, NA = 0.5, E = 20 μJ, and specimen diameter 100 μm. The average specimen velocity during the first 4 μs is about 50 m/s in (A) and 100 m/s in (B). The rotational movement of the specimen in (B) corresponds to a frequency of 600,000 rps during the first microsecond and 330,000 rps when averaged over the first 4 μs.

circular cut and a cylindrical splash evolves. The catapulted specimen maintains a flat, disklike shape, without bulging in the center where the laser irradiance and the ablative pressure are highest. The rim of the specimen is accelerated not only by the ablative pressure (which is lower in this region) but also by the cylindrical splash, which is driven by the ablative pressure and associated with a local concentration of kinetic energy. The combined action of ablative pressure and secondary fluid flow results in an approximately homogeneous acceleration of the sample.

By contrast, in focused catapulting (Fig. 23B), the side of the specimen at which the laser focus is located is most strongly accelerated, and the specimen assumes a fast rotational movement. Within 2 μs, it has turned by 360°, corresponding to a rotation frequency of 500,000 rps, similar to the case of catapulting from a dry substrate shown in Fig. 13. The catapulting velocity is larger than with defocused pulses ($v \approx 60$ m/s, averaged over the first 2 μs compared to $v \approx 45$ m/s) because plasma is formed at the laser focus while defocused catapulting is driven by ablation below the threshold for plasma formation.

The dynamics in Fig. 23 shows no obvious advantage of focused catapulting for live-cell retrieval and recultivation. This advantage arises only when PEN foils and cells are covered with a liquid layer such as in Fig. 24. For defocused catapulting, the upper liquid layer now largely suppresses the splash of liquid from the lower layer and the specimen is hardly accelerated at its periphery. The high pressure produced by ablation in the central region of the specimen results in an upward bulging of this region while the rim is tied down by the inertia of the liquid covering the specimen (Fig. 24A). After about 1 μs, the movement of the specimen center is slowed down by these inertial forces while the radial liquid flow in the upper liquid layer that was created during the first microsecond continues and is focused above the specimen center into an upward directed jet. Because this jet flow is faster than the movement of the specimen, it exerts a shear force on the cells. When the specimen rises out of the liquid, after a few microseconds, some fluid stays behind at the specimen's rim. This results in a flow and shear forces opposite to that of the jet flow. The combined action of these successive shear forces is probably responsible for the removal of most of the cells from the specimen that led to the low success rate of recultivation.

The catapulting dynamics induced by laser pulses focused at the periphery of the dissectats is presented in Fig. 24B. Its principal characteristics resemble the sequence of events observed without a liquid layer covering the cells (Fig. 23B). The pressure within the laser plasma is strong enough to immediately remove the upper liquid layer in the vicinity of the laser focus. This ''Moses effect'' gives leeway to the acceleration of the side of the specimen proximal to the laser focus. Within about 1 μs, the specimen has risen out of the culture medium and rotated by 90°, and after about 4 μs, it has propagated a distance of 220 μm (average velocity 55 m/s) and rotated by 180° (rotation frequency 125,000 rps). Because of the rotation, the fluid flow along the cells during the specimen's take off remains weak, and the shear forces acting on the cells are weaker than in the case of

defocused catapulting. On the other hand, centrifugal forces come into play that increase proportional to the distance r from the axis of rotation. After 5–10 μs (not shown), the specimen flies free of any liquid and the rotational movement has been considerably slowed down by air friction.

Both for focused and defocused catapulting, the exact sequence of events varies with the thickness of the liquid layer above the cells (10–50 μm) but still resembles the behavior portrayed in Fig. 24. After removal of the culture medium, the liquid layer thins because of evaporation. The actual thickness on each individual photograph thus depends on the time after removal of the medium when catapulting was performed. The main consequence of an increasing layer thickness is a slowdown of the dynamics both with regard to translational and rotational specimen velocity.

C. Possible Side Effects and Their Minimization

Criteria for successful live-cell catapulting are (1) the fraction of specimens that can be recovered/collected, (2) the percentage of vital cells per specimen, and (3) the recultivation rate. Adverse factors are (1) large variations in the flight trajectories of the specimens; (2) removal of cells from the substrate by mechanical forces; and (3) damage to cells remaining on the substrate by heat, UV irradiation, or mechanical stress. While the flight trajectories were more stable with defocused catapulting, cell loss and damage were less severe when pulses focused at the rim of the specimen were used. These differences are probably due to distinctions in the mechanical effects rather than to dissimilar responses to heat and UV irradiation.

The possible sources for cellular damage by heat and UV radiation are very similar to those for histologic material that were discussed above, with the threshold values presumably being lower for living cells. Note, however, that the threshold doses for UV light-induced DNA damage and cell killing quoted in Section III.C.2 from the work of de With and Greulich (1995) and Bertling *et al.* (1996) already refer to populations of living cells. The thresholds for thermal cell damage are high for the short heat exposure times involved in catapulting, which last only a few microseconds (see Section III.C.1). Simanowski *et al.* (2005) reported that cells survived temperatures as high as 180°C for heat exposure time of 300 μs. For heat pulses shorter than 300 μs, the threshold for cellular death was determined by the threshold for explosive vaporization that occurred at temperatures slightly above 200°C. Thus, the most likely sources of cell damage in catapulting are mechanical effects. They may result in removal of cells from the membrane, immediate cell lysis, or in more subtle damage to cell membranes and/or organelles.

Looking at the vigorous dynamics portrayed in Figs. 23 and 24, it is quite remarkable that a large number of catapulted cells continue to proliferate in an apparently unimpeded fashion. However, it needs to be kept in mind that rapid motions per se do not necessarily cause damage. Any fluid motion can be decomposed in uniform translation, rigid rotation, and an extensional flow, and only the

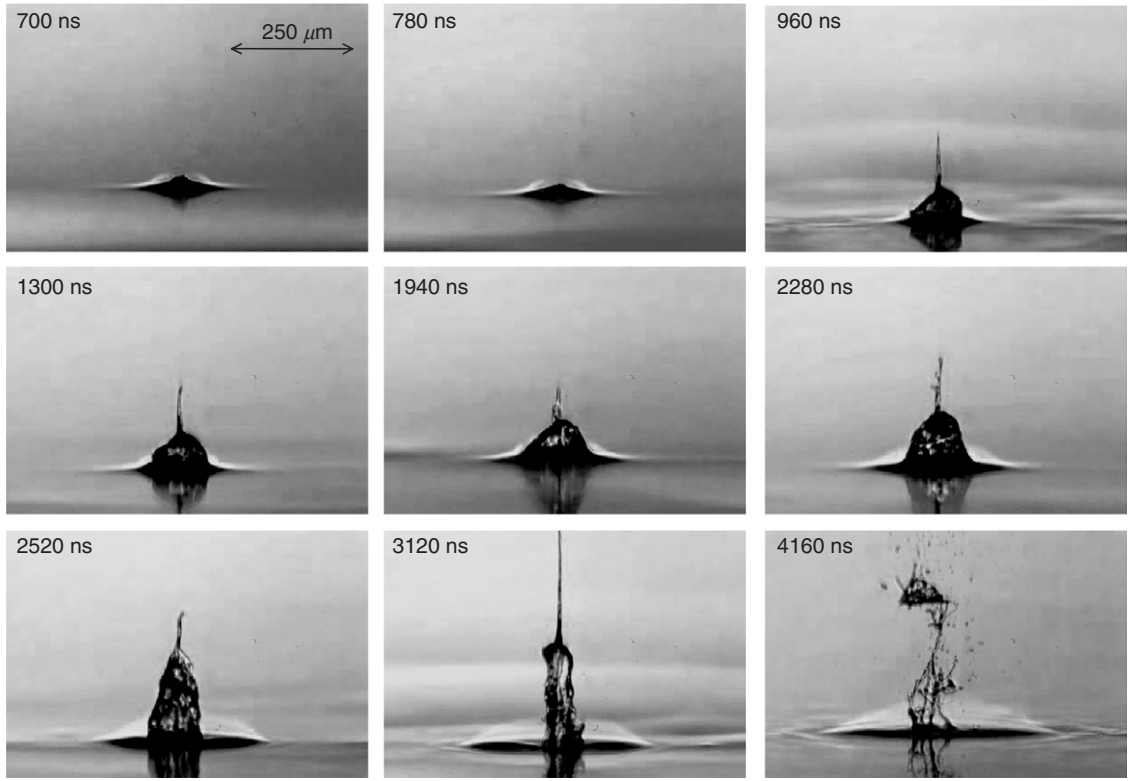
A
700 ns
250 μm
780 ns
960 ns
1300 ns
1940 ns
2280 ns
2520 ns
3120 ns
4160 ns

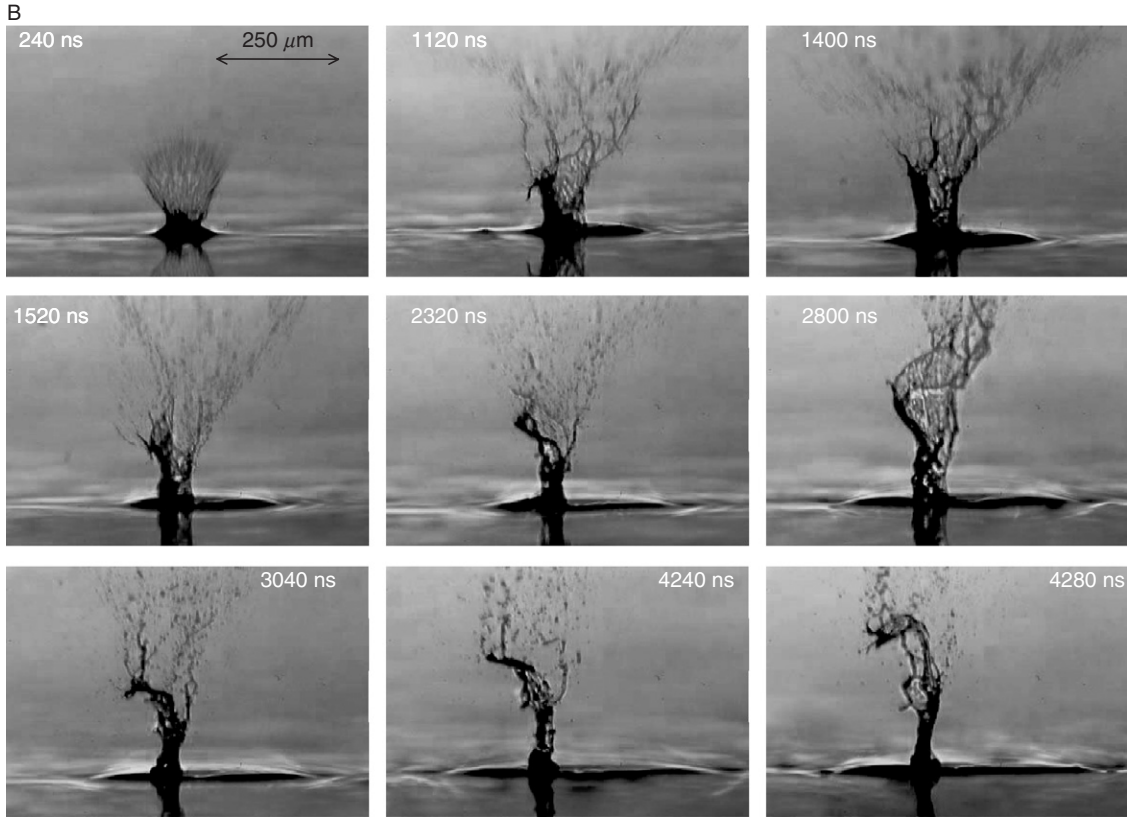

Fig. 24 Catapulting of cell preparations (CHO cells on PEN foil) out of a duplex dish. The liquid layer between Teflon membranes and PEN foil was 30- to 50-μm thick, and a 10- to 50-μm-thick layer of culture medium covered the cells. (A) Catapulting with defocused laser pulses and (B) catapulting with pulses focused at the periphery of the specimen (the plasma luminescence indicates the location of the laser focus). 20$\times$ objective, NA = 0.5, E = 20 μJ, and specimen diameter 100 μm. The average specimen velocity during the first 4 μs is about 50 m/s in (A) and 55 m/s in (B). The rotational movement of the specimen in (B) corresponds to a frequency of 220,000 rps during the first microsecond and 125,000 rps when averaged over the first 4 μs.

latter bears damage potential. Extensional flow patterns associated with tensile stress arise from shear through pressure gradients, inertial or viscous drag, from radial expansion movements (Lokhandwalla and Sturtevant, 2001; Lokhandwalla *et al.*, 2001), or from thermoelastic effects (Paltauf and Dyer, 2003; Vogel and Venugopalan, 2003). With moderately defocused laser pulses, the irradiance is largest in the specimen center. Therefore, the initial pressure distribution is inhomogeneous, and the center of the specimen will bulge upward before it flies off due to the expansion of the bubble below the specimen. The resulting tensile stress and strain may lead to cell detachment or membrane rupture. For later phases of the catapulting dynamics the image series in Figs. 23 and 24 suggest that shear forces are also more pronounced in catapulting with a defocused rather than with a focused laser beam.

However, catapulting with pulses focused at the specimen's rim is associated with a fast rotation of the specimens that gives rise to considerable centrifugal forces that are not observed in defocused catapulting. The initial rotational velocity at the rim of a specimen with 100-μm diameter revolving by 180° in 4 μs such as in Fig. 24B is ≈39 m/s, and the centripetal acceleration $a = v^2/r$ at the specimen rim ($r = 50$ μm) amounts to 3×10^7 m/s^2 for $\nu_R = 125{,}000$ rps. Amazingly, the majority of the cells remain on the specimen in spite of the strong centrifugal force, probably due to its very short duration. Air friction rapidly decelerates the rotational movement, and correspondingly the centrifugal force $F = mv^2/r$ drops very fast such that strong centrifugal forces act only during a few microseconds. This time interval is apparently short enough to allow for elastic deformation avoiding rupture or detachment of cells that are located sufficiently close to the rotation axis as shown in Fig. 22A. However, Fig. 22A also indicates that cells far away from the rotation axis are sheared off—not only in the vicinity of the laser shot but also at the opposite side of the specimen rim.

In general, the damage potential of hydrodynamic effects is not only determined by the magnitude of the tensile or shear forces but also by their duration because the material must be strained before it can rupture. Rupture (or at least poration) of the cell membrane requires an areal strain larger than 2–3% (Boal, 2002; Evans *et al.*, 1976; Needham and Nunn, 1990). The deforming force must last sufficiently long to achieve this deformation. Moreover, the ultimate tensile strength (UTS) of the cell membrane or elements of the cytoskeleton may depend on the strain rate. It has been observed for tissue that, while the strain at fracture does not change significantly with strain rate, the UTS increases. The increase of the UTS is due to the fact that, under conditions of rapid deformation, there is significant viscous dissipation between matrix elements, for example collagen fibrils, and ground substance (Vogel and Venugopalan, 2003; Section II.B). It is conceivable that similar laws also apply on the cellular level. The response of cells to very large strain rates acting for very short time is still largely unexplored and requires further investigation.

Improvements of defocused catapulting can probably be achieved with stronger defocusing and a more homogeneous irradiance distribution at the specimen than

in our present experiments. However, even then the advantage of the rotational movement associated with focused catapulting may still prevail if the liquid layer above the cells is relatively thick. With decreasing thickness of this layer, the catapulting dynamics will change from the scenario shown in Fig. 24A toward that of Fig. 23A which is most likely correlated with less collateral damage.

We observed that a thin liquid layer between Teflon membrane and PEN foil facilitates catapulting. However, it increases the energy requirements for cutting and thus the amount of side effects associated with dissection when it becomes too thick. The optimum thickness of this layer, which may vary with specimen size, still needs to be identified.

V. Conclusions and Outlook

A. Potential Improvements for Dissection

Three different measures can lead to finer dissections than possible with the N_2 laser employed in our experiments: (1) improvement of the beam profile, (2) reduction of the laser pulse duration, and (3) increase of the laser repetition rate. The beam profile of diode-pumped frequency-tripled Nd:YAG lasers that are incorporated in the newest generation of most commercial microbeam system is much better than that of the N_2 laser (see Fig. 3). This can lead to a considerable reduction of the focal spot size, optical breakdown energy, and cutting width, provided that the delivery optics to the focusing microscope objective maintains the good beam quality. This goal will not be achieved if the laser beam is simply coupled into the fluorescence beam path that is optimized for homogeneous illumination of the object field but not for focusing of a laser beam. Additional corrections of the spherical aberrations induced in the beam path of the fluorescence illumination are required to provide optimum focusing conditions.

An even larger reduction of the energy threshold for optical breakdown can be reached by employing shorter laser pulse durations (Vogel *et al.*, 1996a, 2005a). We observed that a reduction of the pulse duration from 6 ns to 300 fs reduces the breakdown threshold at NA = 0.9 by a factor of ~100 for UV wavelengths and even more for IR wavelengths (by A. V. and V. H., unpublished results). Use of fs lasers thus creates the potential for nanosurgery on a subcellular level (König *et al.*, 1999, 2005; Vogel *et al.*, 2005a and references therein) and for gentle optotransfection (Tirlapur and König, 2002). Already a moderate reduction of the laser pulse duration to 500 ps in combination with a good beam profile and the use of UV light ($\lambda = 355$ nm) made it possible to selectively dissect microtubules in live cells (Colombelli *et al.*, 2005).

Especially for pulse durations in the ns range, the use of UV laser pulses seems to be advantageous because the energy threshold for plasma formation decreases with decreasing wavelength. We found that the breakdown threshold for 6-ns pulses measured at NA = 0.9 is 16 times smaller for $\lambda = 355$ nm than for $\lambda = 1064$ nm,

and the cavitation bubble size at threshold is even more strongly reduced (by A. V. and V. H., unpublished results). For fs pulses, the breakdown threshold was five times smaller for $\lambda = 355$ nm than for $\lambda = 1064$ nm.

When very small single-pulse energies are used for dissection, a large number of pulses are necessary to complete a cut of finite length. Therefore, the repetition rate of the laser pulses must be sufficiently large (hundreds of hertz to kilohertz) to avoid an impractical prolongation of the processing time.

B. Potential Improvements for Catapulting

The use of ultrashort laser pulses may not only improve dissection but also increase the efficiency of catapulting because (1) the linear absorption of the sample is supplemented by nonlinear mechanisms (photoionization and avalanche ionization) even for defocused laser beams; (2) the thermal expansion velocity of a heated sample increases with decreasing laser pulse duration; and (3) for sufficiently short pulses, large thermoelastic stresses are generated, and phase transitions occur at lower temperatures. All mentioned effects reduce the energy threshold for catapulting.

Nonlinear absorption will probably make it easier to catapult specimens directly from a glass slide without the use of a strongly UV-absorbing foil, and it permits to use any desired laser wavelength. By reducing the optical penetration depth of the laser light, nonlinear absorption eases the energy requirements for catapulting.

We discussed in Section III.B.3 that for strongly defocused pulses thermal expansion of the heated specimen may contribute to catapulting. This contribution increases with decreasing pulse duration (Arnold, 2002, 2003; Tam *et al.*, 1992). If the temperature rise occurs on a shorter time scale than the stress propagation time out of the heated volume, which is also the time required for thermal expansion, large thermoelastic stresses are generated in the layer absorbing the laser energy. Under such "stress confinement" conditions, part of the laser energy is transformed into elastic energy of the heated sample and the release of this energy during the subsequent expansion phase results in a considerably larger detachment velocity than mere thermal expansion.

In LPC, the light-absorbing layer is located at the bottom of the specimen that is attached to the supporting glass slide. Therefore, the detachment through thermoelastic mechanisms does not occur immediately but with a certain delay: The compressive wave generated in the absorbing layer first travels to the upper side of the specimen bordered by air. Here it is reflected as tensile stress wave because the acoustic impedance of air is much smaller than that of the specimen (Paltauf and Dyer, 2003). This tensile wave travels back into the sample, and when, after a few nanoseconds, it reaches the interface between sample and supporting substrate, it will induce or facilitate the sample's lift off from the substrate. Moreover, the tensile stress wave will reduce the temperature required for explosive vaporization in the heated layer at the bottom of the sample (Vogel and Venugopalan, 2003; Vogel *et al.*, 2005a). The latter effect increases the driving force of phase transitions involved in catapulting.

For biological materials with a sound velocity similar to that of water (1500 m/s) and for an optical penetration depth of, for example 1 μm, the stress confinement condition is fulfilled if the laser pulse duration $t_m \leq 700$ ps. In this case, the degree of stress confinement is small for ns pulses but very high for fs pulses, and it is therefore expected that the catapulting efficiency is better with fs pulses.

Indirect experimental evidence for the above considerations has been provided by Lazare *et al.* (2005) who demonstrated surface foaming of collagen and other biopolymers induced by ablation in the stress confinement regime. We were able to catapult histologic specimens 120 μm in diameter using focused IR fs pulses ($\lambda = 1040$ nm) of only 1.2 μJ (by A. V. and V. H., unpublished results). The corresponding radiant exposure averaged over the entire specimen area is only 0.01 J/cm^2, that is, one-third of the lowest value achieved with UV ns pulses (Table II). Laser printing of biomaterial with fs pulses has been demonstrated by Zergioti *et al.* (2005), and it was shown that the printing process has a better forward directionality with fs pulses than with ns pulses (Papazoglou *et al.*, 2002; Zergioti *et al.*, 2003).

It would be desirable to establish catapulting techniques for histologic samples that do not require a UV absorbing polymer foil because the foil scatters and fluoresces (see Fig. 6B) and thus impairs histochemical and fluorescence identification techniques for cells of interest. It does not help to simply omit the foil because a narrow grid of laser spots is required to catapult the specimens directly from a glass slide, which considerably increases the amount of UV-light induced and thermal damage (see Section III.C). Therefore, new types of dynamic release layers allowing for gentle catapulting will have to be explored. This research may profit from previous experience gathered in the field of laser color printing (Tolbert *et al.*, 1993), laser printing of biomaterials (Colina *et al.*, 2006), laser cleaning (Luk'yanchuk, 2002), polymers especially designed for laser ablation (Lippert *et al.*, 2003), and other fields of laser-mediated mass transfer (Barron *et al.*, 2004; Christescu *et al.*, 2004; Mathews *et al.*, 2006; Wu *et al.*, 2003).

With regard to live-cell catapulting, there is probably even more room for further improvements than with respect to LPC of histologic material. Due to the large number of layers involved in the present technique (Fig. 18), many parameters determine the catapulting dynamics. Among those, the laser spot size, laser energy, and the thickness of both liquid layers (below the PEN foil and above the cells) are especially important. On the basis of a better understanding of the complex sequence fluid dynamics induced by the laser pulse, one will be able to optimize these parameters or to develop alternative catapulting techniques. For reliable and gentle catapulting, the thickness of the liquid layer above the cells should be as small as possible without desiccation of the cells and as reproducible as possible.

Acknowledgments

This work was performed in collaboration with PALM Microlaser Technologies which provided the microbeam system. It was sponsored by the German Bundesministerium für Bildung und Forschung (BMBF) under grant number 13N8461, and, in parts, by US Air Force Office of Scientific Research under grants number FA8655-02-1-3047 and FA8655-05-1-3010. We appreciate stimulating discussions with Karin Schütze, Bernd Sägmüller, and Yilmaz Niyaz of PALM Microlaser Technologies, with Heyke Diddens (Institute of Biomedical Optics, University of Lübeck) who also provided the CHO cell line used for live-cell catapulting, and with Dorthe von Smolinski (Institute of Anatomy, University of Lübeck) who gave valuable advise on real-time RT-PCR. The laser beam profiles of Fig. 3 were provided by Carsten Lüthy (PALM), and the measurements of the thermal properties of polymer foils and histologic specimens quoted in Fig. 4 and Table I were performed by Christine Mimler (Institut für Werkstoffwissenschaften, Universität Erlangen-Nürnberg). We thank Sebastian Freidank, Ingo Apitz, Pieternel Doeswijk, Nadine Steiner, Florian Wölbeling, Helge Meyer, and Reinhard Schulz for technical assistance.

References

Abrahamsen, H. N., Steiniche, T., Nexo, E., Hamilton-Dutoit, S. J., and Sorensen, B. S. (2003). Towards quantitative mRNA analysis in paraffin-embedded tissues using real-time reverse transcriptase-polymerase chain reaction: A methodological study on lymph nodes from melanoma patients. *J. Mol. Diagn.* **5,** 34–41.

Ai, J., Tan, Y., Ying, W., Hong, Y., Liu, S., Wu, M., Qian, X., and Wang, H. (2006). Proteome analysis of hepatocellular carcinoma by laser capture microdissection. *Proteomics* **6,** 538–546.

Amy, R. L., and Storb, R. (1965). Selective mitochondrial damage by a ruby laser microbeam: An electron microscopic study. *Science* **150,** 756–758.

Anderholm, N. C. (1970). Laser-generated stress waves. *Appl. Phys. Lett.* **16,** 113–115.

Apitz, I., and Vogel, A. (2005). Material ejection in nanosecond Er:YAG laser ablation of water, liver, and skin. *Appl. Phys. A* **81,** 329–338.

Arnold, N. (2002). Dry laser cleaning of particles by nanosecond pulses: Theory. *In* "Laser Cleaning" (B. Luk'yanchuk, ed.), pp. 51–102. World Scientific Publishing, Singapore.

Arnold, N. (2003). Theoretical description of dry laser cleaning. *Appl. Surf. Sci.* **208–209,** 15–22.

Ashkin, A. (1986). Observation of a single beam gradient force trap for dielectric particles. *Opt. Lett.* **11,** 288–290.

Barron, J. A., Wu, P., Ladouceur, H. D., and Ringeisen, B. R. (2004). Biological laser printing: A novel technique for creating heterogeneous 3-dimensional cell patterns. *Biomed. Microdevices* **6,** 139–147.

Bäuerle, D. (2000). "Laser Processing and Chemistry," 3rd edn. Spinger-Verlag, Berlin, Heidelberg, New York.

Berns, M. W., Cheng, W. K., Floyd, A. D., and Ohnuki, Y. (1971). Chromosome lesions produced with an argon laser microbeam without dye sensitization. *Science* **171,** 903–905.

Berns, M. W., Olson, R. S., and Rounds, D. E. (1969). *In vitro* production of chromosomal lesions with an argon laser microbeam. *Nature* **221,** 74–75.

Bertling, C. D., Lin, F., and Girotti, A. W. (1996). Role of hydrogen peroxide in the cytotoxic effects of UVA/B radiation on mammalian cells. *J. Photochem. Photobiol.* **64,** 137–142.

Bessis, M., Gires, F., Mayer, G., and Nomarski, G. (1962). Irradiation des organites cellulaires à l'aide d'un laser à rubis. *C. R. Acad. Sci. III-Vie* **255,** 1010–1012.

Boal, D. (2002). "Mechanics of the Cell." Cambridge University Press, Cambridge, UK.

Bustin, S. A. (2000). Absolute quantification of mRNA using real-time reverse transcription polymerase chain reaction assays. *J. Mol. Endocrinol.* **25,** 169–193.

Carslaw, H. S., and Jaeger, J. C. (1959). "Conduction of Heat in Solids," 2nd edn. Oxford University Press, Oxford.

Cheong, W. F., Prahl, S. A., and Welch, A. J. (1990). A review of the optical properties of biological tissue. *IEEE. J. Quantum Electron.* **26,** 2166–2185.

Chrisey, D. B., Piqué, A., McGill, R. A., Horwitz, J. S., Ringeisen, B. R., Bubb, D. M., and Wu, P. K. (2003). Laser deposition of polymer and biomaterial films. *Chem. Rev.* **103,** 553–576.

Christescu, R., Mihaiescu, D., Socol, G., Stamatin, I., Mihailescu, I. N., and Chrisey, D. B. (2004). Deposition of biopolymer thin films by matrix-assisted pulsed laser evaporation. *Appl. Phys. A* **79,** 1023–1026.

Colina, M., Duocastella, M., Fernández-Pradas, J. M., Serra, P., and Morenza, J. L. (2006). Laser-induced forward transfer of liquids: Study of the droplet ejection process. *J. Appl. Phys.* **99,** 084909.

Colombelli, J., Reynaud, E. G., Rietdorf, J., Pepperkork, R., and Stelzer, E. H. K. (2005). Pulsed UV laser nanosurgery: Retrieving the cytoskeleton dynamics *in vivo*. *Traffic* **6,** 1093–1102.

Coohill, T. P. (2002). Uses and effects of ultraviolet radiation on cells and tissues. *In* "Lasers in Medicine" (R. W. Waynant, ed.), pp. 85–107. CRC Press, Boca Raton, London, New York, Washington, DC.

de With, A., and Greulich, K. O. (1995). Wavelength dependence of laser-induced DANN damage in lymphocytes observed by single-cell gel electrophoressis. *J. Photochem. Photobiol. B Biol.* **30,** 71–76.

Dingus, R. S. (1992). Laser-induced contained vaporization in tissue. *Proc. SPIE* **1646,** 266–274.

Dingus, R. S. (1993). Momentum induced by laser-tissue interaction. *Proc. SPIE* **1882,** 399–411.

Eltoum, I. A., Siegal, G. P., and Frost, A. R. (2002). Microdissection of histologoc sections: Past, present, and future. *Adv. Anat. Pathol.* **9,** 316–322.

Elvers, D., Remer, L., Arnold, N., and Bäuerle, D. (2005). Laser microdissection of biological tissues: Process optimization. *Appl. Phys. A* **80,** 55–59.

Emmert-Buck, M. R., Bonner, R. F., Smith, P. D., Chuaqui, R. F., Zhuang, Z., Goldstein, S. R., Weiss, R. A., and Liotta, L. A. (1996). Laser capture microdissection. *Science* **274,** 998–1001.

Ernst, G., Melle, C., Schimmel, B., Bleul, A., and von Eggeling, F. (2006). Proteohistography—direct analysis of tissue with high sensitivity and high spatial resolution using ProteinChip technology. *J. Histochem. Cytochem.* **54,** 13–17.

Evans, E. A., Waugh, R., and Melnik, L. (1976). Elastic are compressibility modulus of red cell membrane. *Biophys. J.* **16,** 585–595.

Fabbro, R., Fournier, J., Ballard, P., Devaux, D., and Virmont, J. (1990). Physical study of laser-produced plasma in confined geometry. *J. Appl. Phys.* **68,** 775–784.

Fairand, B. P., and Clauer, A. H. (1979). Laser-generation of high-amplitude stress waves in materials. *J. Appl. Phys.* **50,** 1497–1502.

Fink, L., Kwapiszewska, G., Wilhelm, J., and Bohle, R. M. (2006). Laser-microdissection for cell type- and compartment-specific analyses on genomic and proteomic level. *Exp. Toxicol. Pathol.* **57**(Suppl. 2), 25–29.

Freund, D. E., McCally, R. L., Farrell, R. A., and Sliney, D. H. (1996). A theoretical comparison of retinal temperature changes resulting from exposure to rectangular and Gaussian beams. *Lasers Life Sci.* **7,** 71–89.

Greulich, K. O. (1999). "Micromanipulation by Light in Biology and Medicine." Birkhäuser, Basel, Boston, Berlin.

Greulich, K. O., and Pilarczyk, G. (1998). Laser tweezers and optical microsurgery in cellular and molecular biology. Working principles and selected applications. *Cell. Mol. Biol.* **44,** 701–710.

Gulmann, C., Espina, V., Petricoin, E., III, Longo, D. L., Santi, M., Knutsen, T., Raffeld, M., Jaffe, E. S., Liotta, L. A., and Feldman, A. L. (2005). Proteomic analysis of apoptotic pathways reveals prognostic factors in follicular lymphoma. *Clin. Cancer Res.* **11,** 5847–5855.

Hibst, R. (1996). "Technik, Wirkungsweise und medizinische Anwendungen von Holmium- und Erbium-Lasern." Ecomed, Landsberg (in German).

Hockberger, P. E., Skimina, T. A., Centonze, V. E., Lavin, C., Chu, S., Dadras, S., Reddy, J. K., and White, J. G. (1999). Activation of flavin-containing oxidases underlies light-induced production of H_2O_2 in mammalian cells. *Proc. Natl. Acad. Sci. USA* **96,** 6255–6260.

Hopp, B., Smausz, T., Kresz, N., Barna, N., Bor, Z., Kolozsvari, L., Chrisey, D. B., Szabo, A., and Nogradi, A. (2005). Survival and proliferative ability of various living cell types after laser-induced forward transfer. *Tissue Eng.* **11,** 1817–1823.

Hosokawa, Y., Takabayashi, H., Miura, S., Shukunami, C., Hiraki, Y., and Masuhara, H. (2004). Nondestructive isolation of single cultured animal cells by femtosecond laser-induced shockwave. *Appl. Phys. A* **79,** 795–798.

Huttmann, G., and Birngruber, R. (1999). On the possibility of high-precision photothermal micro-effects and the measurement of fast thermal denaturation of proteins. *IEEE J. Sel. Topics Quantum Electron.* **5,** 954–962.

Isenberg, G., Bielser, W., Meier-Ruge, W., and Remy, E. (1976). Cell surgery by laser micro-dissection: A preparative method. *J. Microsc.* **107,** 19–24.

Jacques, S. L. (1993). Role of tissue optics and pulse duration on tissue effects during high-power laser irradiation. *Appl. Opt.* **32,** 2447–2454.

Jiménez, J. L., del Valle, G., and Campos, I. (2005). A cononical treatment of some systems with friction. *Europ. J. Phys.* **26,** 711–725.

Karaiskou, A., Zergioti, I., Fotakis, C., Kapsetaki, M., and Kafetzopoulos, D. (2003). Microfabrication of biomaterials by the sub-ps laser-induced forward transfer process. *Appl. Surf. Sci.* **208–209,** 245–249.

Kehr, J. (2003). Single cell technology. *Curr. Opin. Plant Biol.* **6,** 617–621.

König, K., Riemann, I., Fischer, P., and Halbhuber, K. (1999). Intracellular nanosurgery with near infrared femtosecond laser pulses. *Cell. Mol. Biol.* **45,** 195–201.

König, K., Riemann, I., Stracke, F., and Le Harzic, R. (2005). Nanoprocessing with nanojoule near-infrared femtosecond pulses. *Med. Laser Appl.* **20,** 169–184.

Koulikov, S. G., and Dlott, D. D. (2001). Ultrafast microscopy of laser ablation of refractory materials: Ultra low threshold stress-induced ablation. *J. Photochem. Photobiol. A* **145,** 183–194.

Krafft, A. E., Duncan, B. W., Bijwaard, K. E., Taubenberger, J. K., and Lichy, J. H. (1997). Optimization of the isolation and amplification of RNA from formalin-fixed, paraffinembedded tissue: The armed forces institute of pathology experience and literature review. *Mol. Diagn.* **2,** 217–230.

Kuchling, H. (1991). ''Taschenbuchder Physik,'' Fachbuch-Verlag GmbH, Leipzig.

Lahr, G. (2000). RT-PCR from archival single cells is a suitable method to analyze specific gene expression. *Lab. Invest.* **80,** 1477–1479.

Landau, L. D., and Lifschitz, E. M. (1987). ''Fluid Mechanics,'' 2nd edn. Pergamon Press, Oxford.

Lazare, S., Tokarev, V., Sionkowska, A., and Wisniewski, M. (2005). Surface foaming of collagen, chitosan and other biopolymer films by KrF excimer laser ablation in the photomechanical regime. *Appl. Phys. A* **81,** 465–470.

Lee, I.-Y. S., Tolbert, W. A., Dlott, D. D., Doxtader, M. M., Foley, D. M., Arnold, D. R., and Ellis, E. W. (1992). Dynamics of laser ablation transfer imaging investigated by ultrafast microscopy. *J. Imaging Sci. Technol.* **36,** 180–187.

Lewis, F., Maughan, N. J., Smith, V., Hillan, K., and Quirke, P. (2001). Unlocking the archive—gene expression in paraffin-embedded tissue. *J. Pathol.* **195,** 66–71.

Lippert, T., Hauer, M., Phipps, C. R., and Wokaun, A. (2003). Fundamentals and applications of polymers designed for laser ablation. *Appl. Phys. A* **77,** 259–264.

Litjens, R. A. J., Quickenden, T. I., and Freeman, C. G. (1999). Visible and near-ultraviolet absorption spectrum of liquid water. *Appl. Opt.* **38,** 1216–1223.

Lokhandwalla, M., McAteer, J. A., Williams, J. C., Jr., and Sturtevant, B. (2001). Mechanical haemolysis in shock wave lithotripsy (SWL): II. *In vitro* cell lysis due to shear. *Phys. Med. Biol.* **46,** 1245–1264.

Lokhandwalla, M., and Sturtevant, B. (2001). Mechanical haemolysis in shock wave lithotripsy (SWL): I. Analysis of cell deformation due to SWL flow-fields. *Phys. Med. Biol.* **46,** 413–437.

Lorenz, K. (2004). Mechanismen des Katapultierens biologischer Strukturen mit UV-Laserpulsen. Diploma thesis, University of Applied Science Lübeck (in German)Accessible through. Accessible through vogel@bmo.uni-luebeck.de.

Luk'yanchuk, B. (ed.) (2002). "Laser Cleaning." World Scientific Publishing, Singapore.
Mathews, S. A., Augeung, C. Y., and Piqué, A. (2006). Use of Laser Direct Write in microelectronics assembly. *In* "Online Proceedings of LAMP2006. The 4th Int. Congr. Laser Advanced Materials Processing," May 16–19, 2006. Kyoto, Japan, paper 06–19. JLPS–Japan Laser Processing Society.
Mayer, A., Stich, M., Brocksch, D., Schütze, K., and Lahr, G. (2002). Going *in vivo* with laser microdissection. *Methods Enzymol.* **356,** 25–33.
Meier-Ruge, W., Bielser, W., Remy, E., Hillenkamp, F., Nitsche, R., and Unsöld, R. (1976). The laser in the Lowry technique for microdissection of freeze-dried tissue slices. *Histochem J.* **8,** 387–401.
Meredith, G. D., Sims, C. E., Soughayer, J. S., and Allbritton, N. L. (2000). Measurement of kinase activation in single mammalian cells. *Nat. Biotechnol.* **18,** 309–312.
Nahen, K., and Vogel, A. (1996). Plasma formation in water by picosecond and nanosecond Nd:YAG laser pulses—Part II: Transmission, scattering, and reflection. *IEEE J. Sel. Topics Quantum Electron.* **2,** 861–871.
Nakata, Y., and Okada, T. (1999). Time-resolved microscopic imaging of the laser-induced forward transfer process. *Appl. Phys. A* **69**(Suppl.), S275–S278.
Needham, D., and Nunn, R. S. (1990). Elastic deformation and failure of liquid bilayer membranes containing cholesterol. *Biophys. J.* **58,** 997–1009.
Nettikadan, S., Radke, K., Johnson, J., Xu, J., Lynch, M., Mosher, C., and Henderson, E. (2006). Detection and quantification of protein biomarkers from fewer than 10 cells. *Mol. Cell. Proteomics* **5,** 895–901.
Neumann, J., and Brinkmann, R. (2005). Boiling nucleation on melanosomes and microbeads transiently heated by nanosecond and microsecond laser pulses. *J. Biomed. Opt.* **10,** 024001.
Niemz, M. H., Klancnik, E. G., and Bille, J. F. (1991). Plasma-mediated ablation of corneal tissue at 1053 nm using a Nd:YLF oscillator/regenerative amplifier laser. *Lasers Surg. Med.* **11,** 426–431.
Niyaz, Y., Stich, M., Sagmüller, B., Burgemeister, R., Friedemann, G., Sauer, U., Gangnus, R., and Schütze, K. (2005). Noncontact laser microdissection and pressure catapulting: Sample preparation for genomic, transcriptomic, and proteomic analysis. *Methods. Mol. Med.* **114,** 1–24.
Paltauf, G., and Dyer, P. (2003). Photomechanical processes and effects in ablation. *Chem. Rev.* **103,** 487–518.
Papazoglou, D. G., Karaiskou, A., Zergioti, I., and Fotakis, C. (2002). Shadowgraphic imaging of the sub-ps laser-induced forward transfer process. *Appl. Phys. Lett.* **81,** 1594–1596.
Pearce, J., and Thomsen, S. (1995). Rate process analysis of thermal damage. *In* "Optical-Thermal Response of Laser-Irradiated Tissue" (A. J. Welch, and M. Van Germert, eds.), pp. 561–606. Plenum Press, New York.
Phipps, C. R., Reilly, J. P., and Campbell, J. W. C. (2000). Optimum parameters for laser launching objects into low Earth orbit. *Laser Part. Beams* **18,** 661–695.
Phipps, C. R., Turner, T. P., Harrison, R. F., York, G. W., Osborne, W. Z., Anderson, G. K., Corlis, X. F., Haynes, L. C., Steele, H. S., Spicochi, K. C., and King, T. R. (1988). Impulse coupling to targets in vacuum by KrF, HF and CO_2 lasers. *J. Appl. Phys.* **64,** 1083–1096.
Rau, K. R., Guerra, A., Vogel, A., and Venugopalan, V. (2004). Investigation of laser-induced cell lysis using time-resolved imaging. *Appl. Phys. Lett.* **84,** 2940–2942.
Rau, K. R., Quinto-Su, P. A., Hellman, A. N., and Venugopalan, V. (2006). Pulsed laser microbeam-induced cell lysis: Time-resolved imaging and analysis of hydrodynamic effects. *Biophys. J.* **91,** 317–329.
Ready, J. F. (1971). "Effects of High Power Laser Radiation." Academic Press, Orlando.
Ringeisen, B. R., Kim, H., Barron, J. A., Krizman, D. B., Chrisey, D. B., Jackman, S., Auyeung, R. Y. C., and Spargo, B. J. (2004). Laser printing of pluripotent embryonal carcinoma cells. *Tissue Eng.* **10,** 483–491.
Romain, J. P., and Darquey, P. (1990). Shock waves and acceleration of thin foils by laser pulses in confined plasma interaction. *J. Appl. Phys.* **68,** 1926–1928.

Sasnett, M. W. (1989). Propagation or multimode laser beams—the M^2 factor. *In* "The Physics and Technology of Laser Resonators" (D. R. Hall, and P. E. Jackson, eds.), pp. 132–142. Adam Hilger, Bristol, New York.

Schütze, K., and Clement-Sengewald, A. (1994). Catch and move—cut or fuse. *Nature* **368,** 667–668.

Schütze, K., and Lahr, G. (1998). Identification of expressed genes by laser-mediated manipulation of single cells. *Nat. Biotechnol.* **16,** 737–742.

Schütze, K., Pösl, H., and Lahr, G. (1998). Laser micromanipulation systems as universal tools in molecular biology and medicine. *Cell. Mol. Biol.* **44,** 735–746.

Serra, P., Colina, M., Fernández-Pradas, J. M., Sevilla, L., and Morenza, J. L. (2004). Preparation of functional DNA microarrays through laser-induced forward transfer. *Appl. Phys. Lett.* **85,** 1639–1641.

Sheffield, S. A., Rogers, J. W., and Castaneda, J. N. (1986). Velocity measurements of laser-driven flyers backed by high impedance windows. *In* "Shock Waves in Condensed Matter" (Y. M. Gupta, ed.), pp. 541–546. Plenum Press, New York, London.

Siegmann, A. E., Sasnett, M. W., and Johnston, T. F., Jr. (1991). Choice of clip levels for beam width measurements using knife-edge techniques. *IEEE J. Quantum Electron.* **27,** 1098–1104.

Simanowski, D., Sarkar, M., Irani, A., O'Connel-Rodwell, C., Contag, C., Schwettman, A., and Palanker, D. (2005). Cellular tolerance to pulsed heating. *Proc. SPIE* **5695,** 254–259.

Sims, C. E., Meredith, G. D., Krasieva, T. B., Berns, M. W., Tromberg, B. J., and Allbritton, N. L. (1998). Laser-micropipet combination for single-cell analysis. *Anal. Chem.* **700,** 4570–4577.

Stanta, G., and Schneider, C. (1991). RNA extracted from paraffin-embedded human tissues is amenable to analysis by PCR amplification. *Biotechniques* **11,**304, 306, 308.

Star, W. M., Marijnissen, J. P. A., and van Gemert, M. J. C. (1988). Light dosimetry in optical phantoms and in tissues. *Phys. Med. Biol.* **33,** 437–454.

Stich, M., Thalhammer, S., Burgemeister, R., Friedemann, G., Ehnle, S., Lüthy, C., and Schütze, K. (2003). Live cell catapulting and recultivation. *Pathol. Res. Pract.* **199,** 405–409.

Stolarski, J., Hardman, J., Bramlette, C. G., Noojin, G. D., Thomas, R. J., Rockwell, B. A., and Roach, W. P. (1995). Integrated light spectroscopy of laser-induced breakdown in aqueous media. *Proc. SPIE* **2391,** 100–109.

Tam, A. C., Leung, W. P., Zapka, W., and Ziemlich, W. (1992). Laser-cleaning techniques for removal of surface particulates. *J. Appl. Phys.* **71,** 3515–3523.

Thalhammer, S., Lahr, G., Clement-Sengewald, A., Heckl, W. M., Burgemeister, R., and Schütze, K. (2003). Laser microtools in cell biology and molecular medicine. *Laser Phys.* **13,** 681–691.

Tirlapur, U. K., and König, K. (2002). Targeted transfection by femtosecond laser. *Nature* **418,** 290–291.

Tolbert, W. A., Lee, I. Y. S., Doxtader, M. M., Ellis, E. W., and Dlott, D. D. (1993). High-speed color imaging by laser ablation transfer with a dynamic release layer: Fundamental mechanisms. *J. Imaging Sci. Technol.* **37,** 411–421.

Tyrrell, R. M., and Keyse, S. M. (1990). The interaction of UVA radiation with cultured cells. *J. Photochem. Photobiol. B Biol.* **4,** 349–361.

Venugopalan, V., Guerra, A., Nahen, K., and Vogel, A. (2002). The role of laser-induced plasma formation in pulsed cellular microsurgery and micromanipulation. *Phys. Rev. Lett.* **88,** 078103.

Vogel, A., Apitz, I., Freidank, S., and Dijkink, R. (2006). Sensitive high-resolution white-light Schlieren technique with large dynamic range for the investigation of ablation dynamics. *Opt. Lett.* **31,** 1812–1814.

Vogel, A., Busch, S., and Parlitz, U. (1996b). Shock wave emission and cavitation bubble generation by picosecond and nanosecond optical breakdown in water. *J. Acoust. Soc. Am.* **100,** 148–165.

Vogel, A., Dlugos, C., Nuffer, R., and Birngruber, R. (1991). Optical properties of human sclera, and their consequences for transscleral laser applications. *Lasers Surg. Med.* **11,** 331–340.

Vogel, A., Lorenz, K., Apitz, I., Freidank, S., and Horneffer, V. (2007). Laser catapulting of histologic specimens with focused and defocused laser pulses. *Biophys. J.* (submitted for publication).

Vogel, A., Lorenz, K., Sägmüller, B., and Schütze, K. (2005b). Catapulting of microdissected histologic specimens with focused and defocused laser pulses. *Proc. SPIE* **5863,** 8–10.

Vogel, A., Nahen, K., and Theisen, D. (1996a). Plasma formation in water by picosecond and nanosecond Nd:YAG laser pulses—Part I: Optical breakdown at threshold and superthreshold irradiance. *IEEE J. Sel. Topics Quantum Electron.* **2,** 847–860.

Vogel, A., Noack, J., Hüttmann, G., and Paltauf, G. (2005a). Mechanisms of femtosecond laser nanosurgery of cells and tissues. *Appl. Phys. B* **81,** 1015–1047.

Vogel, A., Noack, J., Nahen, K., Theisen, D., Busch, S., Parlitz, U., Hammer, D. X., Nojin, G. D., Rockwell, B. A., and Birngruber, R. (1999). Energy balance of optical breakdown in water at nanosecond to femtosecond time scales. *Appl. Phys. B* **68,** 271–280.

Vogel, A., Schweiger, P., Frieser, A., Asiyo, M., and Birngruber, R. (1990). Intraocular Nd:YAG laser surgery: Light-tissue interaction, damage range, and reduction of collateral effects. *IEEE J. Quantum Electron.* **26,** 2240–2260.

Vogel, A., and Venugopalan, V. (2003). Mechanisms of pulsed laser ablation of biological tissues. *Chem. Rev.* **103,** 577–644.

von Smolinski, D., Blessenohl, M., Neubauer, C., Kalies, K., and Gebert, A. (2006). Validation of a novel ultra-short immuno-labelling method for high quality mRNA preservation in laser microdissection and real-time RT-PCR. *J. Mol. Diagn.* **8,** 246–253.

von Smolinski, D., Leverkoehne, I., von Samson-Himmelstjerna, G., and Gruber, A. D. (2005). Impact of formalin-fixation and paraffin-embedding on the ratio between mRNA copy numbers of differently expressed genes. *Histochem. Cell Biol.* **124,** 177–188.

Wu, P. K., Ringeisen, B. R., Krizman, D. B., Frondoza, C. G., Brooks, M., Bubb, D. M., Auyeung, R. C. Y., Piqué, A., Spargo, B., McGill, R. A., and Chrisey, D. B. (2003). Laser transfer of biomaterials: Matrix-assisted pulsed laser evaporation (MAPLE) and MAPLE Direct Write. *Rev. Sci. Instrum.* **74,** 2546–2557.

Young, D., Auyeung, R. C. Y., Piqué, A., and Chrisey, D. B. (2001). Time-resolved optical microscopy of a laser-based forward transfer process. *Appl. Phys. Lett.* **78,** 3169–3171.

Zergioti, I., Karaiskou, A., Papazoglou, D. G., Fotakis, C., Kapsetaki, M., and Kafetzopoulos, D. (2005). Femtosecond laser microprinting of biomaterials. *Appl. Phys. Lett.* **86,** 163902.

Zergioti, I., Papzoglou, D. G., Karaiskou, A., Fotakis, C., Gamaly, E., and Rode, A. (2003). A comparative Schlieren imaging study between ns and sup-ps laser forward transfer of Cr. *Appl. Surf. Sci.* **208–209,** 177–180.